12836–12854 *Nucleic Acids Research, 2021, Vol. 49, No. 22* *Published online 6 December 2021*
https://doi.org/10.1093/nar/gkab1173

Cockayne syndrome group B protein regulates fork restart, fork progression and MRE11-dependent fork degradation in BRCA1/2-deficient cells

Nicole L. Batenburg[1], Sofiane Y. Mersaoui[2], John R. Walker[1], Yan Coulombe[2], Ian Hammond-Martel[3], Hugo Wurtele[3,4], Jean-Yves Masson[2] and Xu-Dong Zhu[1,*]

[1]Department of Biology, McMaster University, Hamilton, Ontario L8S 4K1, Canada, [2]CHU de Québec-Université Laval, Oncology Division, Department of Molecular Biology, Medical Biochemistry and Pathology, Laval University Cancer Research Center, 9 McMahon, Québec City, Québec G1R 3S3, Canada, [3]Centre de recherche, de l'Hôpital Maisonneuve-Rosemont, 5415 boulevard de l'Assomption, Montréal, Québec H1T 2M4, Canada and [4]Department of Medicine, Université de Montréal, Montréal, Québec H3T 1J4, Canada

Received July 03, 2021; Revised November 08, 2021; Editorial Decision November 10, 2021; Accepted November 30, 2021

ABSTRACT

Cockayne syndrome group B (CSB) protein has been implicated in the repair of a variety of DNA lesions that induce replication stress. However, little is known about its role at stalled replication forks. Here, we report that CSB is recruited to stalled forks in a manner dependent upon its T1031 phosphorylation by CDK. While dispensable for MRE11 association with stalled forks in wild-type cells, CSB is required for further accumulation of MRE11 at stalled forks in BRCA1/2-deficient cells. CSB promotes MRE11-mediated fork degradation in BRCA1/2-deficient cells. CSB possesses an intrinsic ATP-dependent fork reversal activity *in vitro,* which is activated upon removal of its N-terminal region that is known to autoinhibit CSB's ATPase domain. CSB functions similarly to fork reversal factors SMARCAL1, ZRANB3 and HLTF to regulate slowdown in fork progression upon exposure to replication stress, indicative of a role of CSB in fork reversal *in vivo*. Furthermore, CSB not only acts epistatically with MRE11 to facilitate fork restart but also promotes RAD52-mediated break-induced replication repair of double-strand breaks arising from cleavage of stalled forks by MUS81 in BRCA1/2-deficient cells. Loss of CSB exacerbates chemosensitivity in BRCA1/2-deficient cells, underscoring an important role of CSB in the treatment of cancer lacking functional BRCA1/2.

INTRODUCTION

Progression of DNA replication forks can be challenged by both exogenous and endogenous sources of genotoxic stress, including DNA lesions, unusual DNA structures such as G-quadruplex, tightly bound protein–DNA complexes and oncogene activation (1,2). Depending upon the nature and the genomic location of these obstacles, eukaryotic cells proceed with different pathways to continue DNA replication or restart stalled forks, including dormant origin firing, replication fork repriming, translesion synthesis, template switching and fork reversal (3). Replication fork stalling, if not properly addressed, represents a major source of genomic instability that can drive tumorigenesis (2).

Upon stalling, replication forks can reverse their course and this fork reversal involves the coordinated annealing of newly synthesized DNA strands, leading to the formation of four-way structures (4,5). Fork reversal can serve as a protective mechanism, allowing the resumption of DNA synthesis without chromosome breakage (5). Several DNA translocases such as SMARCAL1, ZRANB3, FANCM and HLTF, along with the recombinase RAD51, have been implicated in catalyzing fork reversal (6–12). Nascent DNA strands at reversed forks are vulnerable to nucleolytic degradation and their protection requires the tumor suppressor proteins BRCA1 and BRCA2, germline mutations of which predispose individuals to breast and/or ovarian cancer (13). BRCA1 and BRCA2 block the action of the MRE11 nuclease on nascent DNA strands independently of their well-known role in DNA double-strand break (DSB) repair (6,7,14–19). It has been suggested that extensive resection of nascent strands by MRE11 is a leading cause of chemosensitivity in BRCA1/2-deficient cells (16). However, restoration of fork protection does not always lead to chemoresistance in BRCA1/2-deficient cells in other studies (20,21), underscoring the complexity of the molecular mechanisms that underlie chemotherapy response in BRCA1/2-deficient cells.

*To whom correspondence should be addressed. Tel: +1 905 525 9140 (Ext 27737); Fax: +1 905 522 6066; Email: zhuxu@mcmaster.ca

Persistently stalled or collapsed forks can be processed by MUS81, a structure-specific nuclease, into DSBs (22,23). Recent studies suggest that break-induced replication (BIR), a homologous recombination (HR)-based DSB repair pathway that is dependent upon RAD52 and POLD3, mediates repair of DSBs to restart stalled replication forks (24,25). However, how BIR is regulated in the absence of BRCA1 or BRCA2 to mediate the restart of stalled forks has not been fully characterized.

The Cockayne syndrome group B (CSB) protein, also known as ERCC6, is a multifunctional protein that belongs to the SF2 helicase superfamily. CSB contains a central ATPase domain and its ATPase activity is autoinhibited by its N-terminal region (26). It has been suggested that CSB phosphorylation on S10 and S158 releases the autoinhibitory effect of its N-terminal region on its ATPase activity *in vivo* (27). Although first described for its role in transcription-coupled nucleotide excision repair (28,29), recent studies suggest that CSB plays a role in DNA DSB repair (30–32). CSB remodels chromatin surrounding DSBs to promote the choice of DSB repair pathways toward HR in S/G2 (27,33). In addition, CSB interacts with a number of proteins that have been implicated in the protection and restart of stalled forks (27,31,33,34), including BRCA1, MRE11/RAD50/NBS1, RIF1, RAD52 and PARP-1. CSB promotes HR-mediated repair of DSBs arising from stalled forks at telomeres in ALT cells (32). Cells deficient in CSB are sensitive to a range of replication stress-inducing chemical agents, including camptothecin, cisplatin and olaparib (27,30,33,35,36). However, little is known about the role of CSB in replication stress.

In this report, we have uncovered that CSB is recruited to stalled forks to regulate fork restart, fork progression and fork stability in BRCA1/2-deficient cells. We have shown that CSB catalyzes fork reversal under the condition where the autoinhibition by its N-terminal region is released. CSB promotes slowdown in fork progress upon exposure to a low level of replication stress in a manner similar to SMARCAL1, ZRANB3 and HLTF, each of which is a known fork reversal protein, indicative of a role of CSB in fork reversal *in vivo*. CSB promotes fork degradation in BRCA1/2-deficient cells, likely through both catalyzing fork reversal and recruiting MRE11 to stalled forks. Furthermore, CSB promotes fork restart and RAD52-dependent BIR repair of stalled forks in BRCA1/2-deficient cells. Loss of CSB and BRCA1/2 deficiency are a toxic combination to cell survival in response to replication stress, suggesting that CSB is a promising target in the treatment of cancer lacking functional BRCA1/2.

MATERIALS AND METHODS

Plasmids, siRNA, antibodies and drugs

Retroviral expression constructs of Myc-tagged CSB wild type and mutants (W851R, S10A, S10D, S10A-S158A and S1276A), as well as pDEST-mCherry-LacR-NLS-MRE11, have been described (27,30,33,37). Wild-type CSB was used as a template to generate, via site-directed mutagenesis, CSB mutants (CSB-S1009A, CSB-T1031A, CSB-S1348A and CSB-S10D-S158D). These mutants were then cloned into the retroviral expression vector pLPC-N-Myc (38). The GFP-based BIR reporter plasmid pBIR-GFP (24) (Addgene plasmid # 49807) was a gift from Thanos Halazonetis.

siRNAs used were from Dharmacon: nontargeting siRNA (siControl; D-001206-14-05); siBRCA1 (D-003461-05); siBRCA1-2 (CUAGAAAUCUGUUGCUAUG) (39); siBRCA2 (D-003462-04); siBRCA2-2 (J-003462-05) (40); siCtIP (GCUAAAACAGGAACGAAUC); siBOD1L (J-017033-19); siSMARCAL1 (D-013058-04-0002) (32); siZRANB3 (GAGUUACCUUAUUGUGAAA) (41); siHLTF (GGAAUAUAAUGUUAACGAU) (41); siRAD52 (AAGGAUGGUUCAUAUCAUGAA) (42); and siMUS81 (CAGCCCUGGUGGAUCGAUA). Drugs used were hydroxyurea (HU; BioShop Canada), olaparib (Selleck Chemicals), cisplatin (Sigma), CGP74514A (Sigma), roscovitine (Millipore), mirin (Cayman Chemical) and aphidicolin (BioShop Canada).

The rabbit polyclonal anti-pT1031 antibody was developed by LifeTein against a CSB peptide containing phosphorylated threonine T1031 (TGSDVQ-pT-PKCHLKRR) (LifeTein). Other antibodies used include the following: BRCA1 (07-434, Millipore); BRCA2 (A303-434A, Bethyl Laboratories); CSB (A301-345A, Bethyl Laboratories); CSB (553C5a, Fitzgerald); cyclin A (ab16726, Abcam); Myc (9E10, Calbiochem); MRE11 (43) (a kind gift from John Petrini, Memorial Sloan-Kettering Cancer Center); MUS81 (sc-47692, Santa Cruz); RAD52 (sc-365341, Santa Cruz); biotin (A150-109A, Bethyl Laboratories); biotin (200-002-211, Jackson ImmunoResearch); and γ-tubulin (GTU88, Sigma).

Cell culture, transfection and retroviral infection

All cells were grown in DMEM medium with 10% fetal bovine serum supplemented with nonessential amino acids, L-glutamine, 100 U/ml penicillin and 0.1 mg/ml streptomycin. Cell lines used were as follows: hTERT-RPE parental and CSB knockout (KO) (30), U2OS (ATCC), U2OS CSB-KO (27), U2OS-265 CSB-KO (27), HCT116 (Life Technology), HCT116-CSB-KO (27), HEK293 (ATCC) and Phoenix (44). Cell cultures were routinely fixed, stained with DAPI and examined for mycoplasma contamination. Retroviral gene delivery was carried out as described (45,46) to generate stable cell lines. DNA and siRNA transfections were carried out with respective JetPrime® transfection reagent (Polyplus) and Lipofectamine RNAiMAX (Invitrogen) according to their respective manufacturer's instructions.

PLA assays

Proximity ligation (PLA) assays were performed using Duolink® PLA kit (Sigma) according to the manufacturer's instructions. Briefly, coverslips were blocked in Duolink® blocking solution for 30 min at 37°C, followed by incubation with primary antibody diluted in Duolink® antibody diluent overnight at 4°C. Following washes twice in wash buffer A (0.15 M NaCl, 10 mM Tris–HCl, pH 7.4, 0.05% Tween 20) for 5 min, coverslips were incubated with anti-rabbit PLUS and anti-mouse MINUS PLA probes diluted in Duolink® antibody diluent for 1 h at 37°C. Subsequently, coverslips were washed twice in wash buffer A

for 5 min and then ligated for 30 min at 37°C. Coverslips were then washed twice in wash buffer A for 5 min and amplification was performed using Duolink® *In Situ* Detection Reagents Green for 100 min at 37°C. After amplification, coverslips were washed twice in wash buffer B (0.1 M NaCl, 0.2 M Tris) for 10 min and once in 0.1× wash buffer B for 1 min. Finally, coverslips were stained with DAPI [100 ng/ml in phosphate-buffered saline (PBS)]. Cell images were recorded on a Zeiss Axioplan 2 microscope with a Hamamatsu C4742-95 camera and processed in Open Lab. PLA signals were quantified using ImageJ software (NIH).

DNA fiber analysis

DNA fiber analysis was done essentially as described (47). For fork protection, cells were incubated first with 25 μM IdU (I7125, Sigma) for 20 min and then 250 μM CldU (C6891, Sigma) for 20 min prior to treatment with 4 mM HU for 5 h. For fork restart, cells were incubated with 25 μM IdU for 20 min and then treated with 4 mM HU for 4 h, followed by incubation with 250 μM CldU for 60 min. For fork progression, cells were incubated with 25 μM IdU for 30 min and then 250 μM CldU in the presence or absence of 50 μM HU for 30 min. Following labeling, cells were collected by trypsinization and counted. Cells were then spotted onto one end of a glass slide, lysed in freshly made lysis buffer [50 mM EDTA, pH 8.0, 200 mM Tris–HCl, pH 7.5, 0.5% sodium dodecyl sulfate (SDS)] for 5 min and stretched onto the slide. Slides were then fixed in freshly made methanol–acetic acid (3:1) for 20 min at −20°C and then allowed to air dry. Following incubation in freshly prepared 2.5 M HCl for 80 min, slides were washed three times in PBS and blocked with 5% bovine serum albumin (BSA) in PBS for 20 min at room temperature. Slides were then incubated with both rat anti-BrdU (1:400, NB500-169, Novus Biologicals) and mouse anti-BrdU (1:50, 347580, BD Sciences) antibodies prepared in 5% BSA in PBS for 2 h at room temperature. Subsequently, slides were washed three times in PBS and incubated with both Alexa-488 anti-rat (1:250, 712-545-153, Jackson ImmunoResearch) and Rhodamine anti-mouse (1:250, 715-295-151, Jackson ImmunoResearch) secondary antibodies for 1 h at room temperature. DNA fiber images were recorded on a Zeiss Axioplan 2 microscope with a Hamamatsu C4742-95 camera and processed in Open Lab. DNA fiber analysis was carried out with ImageJ software (NIH).

Immunofluorescence

Immunofluorescence (IF) was performed as described (30,38). To detect EdU, cells seeded on coverslips were treated with 10 μM EdU for 10 min prior to treatment with or without 4 mM HU. Following fixation, cells on coverslips were washed with PBS and then incubated with freshly prepared Click-iT reaction buffer (2 mM $CuSO_4$, 10 μM biotin–PEG3–azide, 10 mM ascorbic acid) for 10 min at room temperature. Coverslips were then washed in PBS twice, followed by regular IF as described (30,38). To detect HU-induced MRE11 foci, cells were pre-extracted with cold CSK buffer (10 mM PIPES, pH 7.0, 100 mM NaCl, 300 mM sucrose, 3 mM $MgCl_2$, 0.7% Triton X-100) for 5 min prior to fixation. All cell images were recorded on a Zeiss Axioplan 2 microscope with a Hamamatsu C4742-95 camera and processed in Open Lab.

GFP reporter assays

U2OS and U2OS CSB-KO cells were transfected with pBIR-GFP, I-SceI and pCherry with a 4.5:4.5:1 ratio. Forty-eight hours after transfection, cells were harvested, fixed and subjected to FACS analysis as described (27,30). Cherry expression was used as a transfection efficiency control. A total of 50,000 events per cell line were scored for each independent experiment. FACS analysis was performed on a BD™ Accuri C6 Plus Flow Cytometer.

Immunoblotting and immunoprecipitation

Immunoblotting and immunoprecipitation were performed as described (33).

Protein purification

CSB-WT, CSB-230 (amino acids 230–1439), CSB-360 (amino acids 360–1439), CSB-447 (amino acids 447–1439), CSB-360-W851R and CSB-S10D-S158D were tagged at the N-terminus with GST and at the C-terminus with His_{10}, expressed in Sf9 insect cells and purified as described (48). Briefly, 400 ml of Sf9 insect cells were infected with CSB or CSB mutant baculoviruses for 3 days at 27°C. The cell pellets were resuspended into a final volume of 50 ml with PBS300 lysis buffer [1× PBS containing 300 mM NaCl, 1 mM EDTA, 0.1 mM DTT, 0.05% Triton X-100 containing protease inhibitors (Roche), aprotinin 0.019 TIU/ml and leupeptin 1 μg/ml]. The suspension was lysed using a Branson Sonifier 250 (30% amplitude, during 2 min, 30 s on, 20 s off). Benzonase (15 U/ml) and $MgCl_2$ (1 mM) were added for 1 h at 4°C and insoluble material was removed by centrifugation (35,000 rpm for 40 min) using Sorvall Ultra Pro 80 T647.5 rotor. One milliliter (slurry) of prewashed GST beads was added to the soluble extract for 1.5 h at 4°C. The beads were washed first briefly with washing buffer PBS300 containing 1 mM DTT, and then during 30 min with PBS300 containing 5 mM ATP and 15 mM $MgCl_2$. Beads were then washed once with PBS containing 500 mM NaCl and 1 mM DTT, and once with P5 Talon buffer (20 mM $NaHPO_4$, pH 7.4, 500 mM NaCl, 10% glycerol, 0.02% Triton, 5 mM imidazole). Proteins were eluted by cleavage with PreScission protease (purified in-house) overnight at 4°C. The eluted proteins were diluted in 10 ml of Talon buffer, and 400 μl (slurry) of Talon resin (Clontech) was added and incubated for 1 h at 4°C. The Talon resin was washed three times with Talon buffer. Proteins were eluted with Talon buffer containing 500 mM imidazole and dialyzed in storage buffer (20 mM Tris–acetate, pH 8.0, 200 mM KOAc, 10% glycerol, 1 mM EDTA, 0.5 mM DTT).

Fork reversal and displacement assays

Fork reversal and displacement assays were carried out as described (12). Briefly, the reaction was performed in buffer containing 25 mM MOPS, pH 7.0, 60 mM KCl, 0.2%

Tween, 2 mM DTT, 5 mM $MgCl_2$, 5 mM ATP, 10% glycerol with 0.5 nM ^{32}P-labeled DNA (see primers in Supplementary Table S1) and purified CSB proteins at the indicated concentration. The reaction mixtures were incubated at 37°C for 10 min, and deproteinized for 10 min with stop buffer containing 2 mg/ml proteinase K and 1% SDS. DNA samples were loaded onto 10% native polyacrylamide gels with 10% glycerol and 0.02% bromophenol blue. The products were separated by electrophoresis using 1× TBE buffer. The gel was then exposed and read using Fujifilm FLA 5100.

Clonogenic survival assays

Clonogenic survival assays were done as described (30).

Statistical analysis

A Student's two-tailed unpaired *t*-test was used to derive all *P*-values except for where specified.

RESULTS

CDK-dependent CSB phosphorylation on T1031 mediates the CSB–MRE11 interaction and is dispensable for DSB break repair

We have previously reported that CSB, via its C-terminal region, interacts with MRE11 in a cell cycle-regulated manner (33). The C-terminal region of CSB contains four CDK consensus pS/TP motifs, $S^{1009}P$, $T^{1031}P$, $S^{1276}P$ and $S^{1348}P$. To investigate whether any of these four potential sites mediate the interaction of CSB with MRE11, we generated Myc-tagged CSB WT or Myc-CSB carrying an alanine mutation at each of these four positions and investigated their interaction with mCherry-LacR-MRE11 at the lac operator arrays in the reporter U2OS-265 CSB-KO cell line (33). The U2OS-265 CSB-KO cell line is derived from the U2OS-265 cell line that carries the 256-copy lac operator integrated into a single site on chromosome 1 (49). In agreement with our previous finding (33), Myc-CSB WT was readily recruited by mCherry-LacR-MRE11 to the lac operator array in U2OS-265 CSB-KO cells (Supplementary Figure S1A). This recruitment was impaired by the T1031A mutation but not by the S1009A, the S1276A or the S1348A mutation (Supplementary Figure S1A). To further investigate whether the T1031A mutation might affect the CSB–MRE11 interaction, we performed coimmunoprecipitation analysis with IgG or an anti-MRE11 antibody in U2OS CSB-KO cells stably expressing Myc-CSB WT or Myc-CSB-T1031A. While MRE11 brought down Myc-CSB, it failed to bring down Myc-CSB-T1031A (Figure 1A). A phospho-antibody raised against a CSB peptide phosphorylated on T1031 (anti-CSB-pT1031) readily recognized Myc-CSB WT but not Myc-CSB-T1031A (Figure 1B). Using this anti-CSB-pT1031 antibody, we were not able to detect endogenous CSB phosphorylated on T1031 (N.L. Batenburg and X.-D. Zhu, unpublished data), which is likely due to a low level of T1031 phosphorylation. We have previously reported that Myc-CSB is highly overexpressed compared to endogenous CSB (50), which likely facilitated the detection of Myc-CSB by the anti-CSB-pT1031 antibody. T1031 phosphorylation was sensitive to treatment with two independent CDK inhibitors roscovitine (CDKi-1) and CGP74514A (CDKi-2) (Figure 1C). Taken together, these results suggest that CDK phosphorylates T1031 of CSB and that this phosphorylation mediates the CSB–MRE11 interaction.

We have previously reported that CSB promotes MRE11 recruitment to IR-induced DSBs to facilitate DNA end resection, enforcing HR as the choice of DNA DSB repair pathway (33). To investigate whether T1031 phosphorylation is required for CSB function in recruiting MRE11 to IR-induced DSBs, we complemented hTERT-RPE CSB-KO cells with the vector alone, Myc-CSB or Myc-CSB-T1031A. We observed that overexpression of Myc-CSB-T1031A fully restored the formation of IR-induced MRE11 foci in hTERT-RPE CSB-KO cells, indistinguishable from overexpression of Myc-CSB WT (Supplementary Figure S1B and C), suggesting that CSB phosphorylation on T1031 is not involved in regulating MRE11 recruitment to DSBs. In addition, overexpression of Myc-CSB-T1031A not only fully restored IR-induced BRCA1 foci formation in hTERT-RPE CSB-KO cells but also suppressed IR-induced RIF1 foci formation in hTERT-RPE CSB-KO cells staining positive for cyclin A, a marker for S/G2 cells (Supplementary Figure S1D and E), suggesting that T1031 phosphorylation is dispensable for CSB's role in regulating DNA DSB repair pathway choice. In support of this notion, Myc-CSB-T1031A fully suppressed the sensitivity of U2OS CSB-KO cells to olaparib (Supplementary Figure S1F), a PARP inhibitor known to be toxic for cells deficient in HR.

CSB is recruited to stalled forks in a manner dependent upon T1031 phosphorylation

Aside from DSBs, MRE11 is also known to be recruited to stalled forks, forming HU-induced foci (51). Therefore, we asked whether CSB might interact with MRE11 at stalled forks. To address this question, we employed a PLA-based assay that measures *in situ* protein interactions with nascent DNA at replication forks, known as SIRF (52). We detected HU-induced PLA foci formation between CSB and MRE11 in hTERT-RPE cells and this CSB–MRE11 PLA foci formation was abrogated by the loss of CSB (Figure 1D and E), suggesting that CSB interacts with MRE11 at stalled forks. HU-induced PLA foci formation was also detected between EdU and either endogenous CSB or exogenously expressed Myc-CSB in cells that were pulse labeled with EdU for 10 min prior to HU treatment (Figure 1F and G, and Supplementary Figure S2A and B), further demonstrating that CSB is associated with stalled forks. PLA foci formation between CSB and either MRE11 or EdU was also observed in cells without HU treatment (Figure 1D–G), indicative of CSB's association with ongoing replication forks, in agreement with a previous report that CSB is detected at DNA replication forks (53).

Further analysis revealed that while treatment with HU increased the Myc-CSB-EdU PLA foci formation, it failed to stimulate the Myc-CSB-T1031A-EdU foci formation (Figure 1H). The Myc-CSB-T1031A mutant was also found to be defective in forming PLA foci with MRE11 at stalled forks (Figure 1I and Supplementary Figure S2C). These

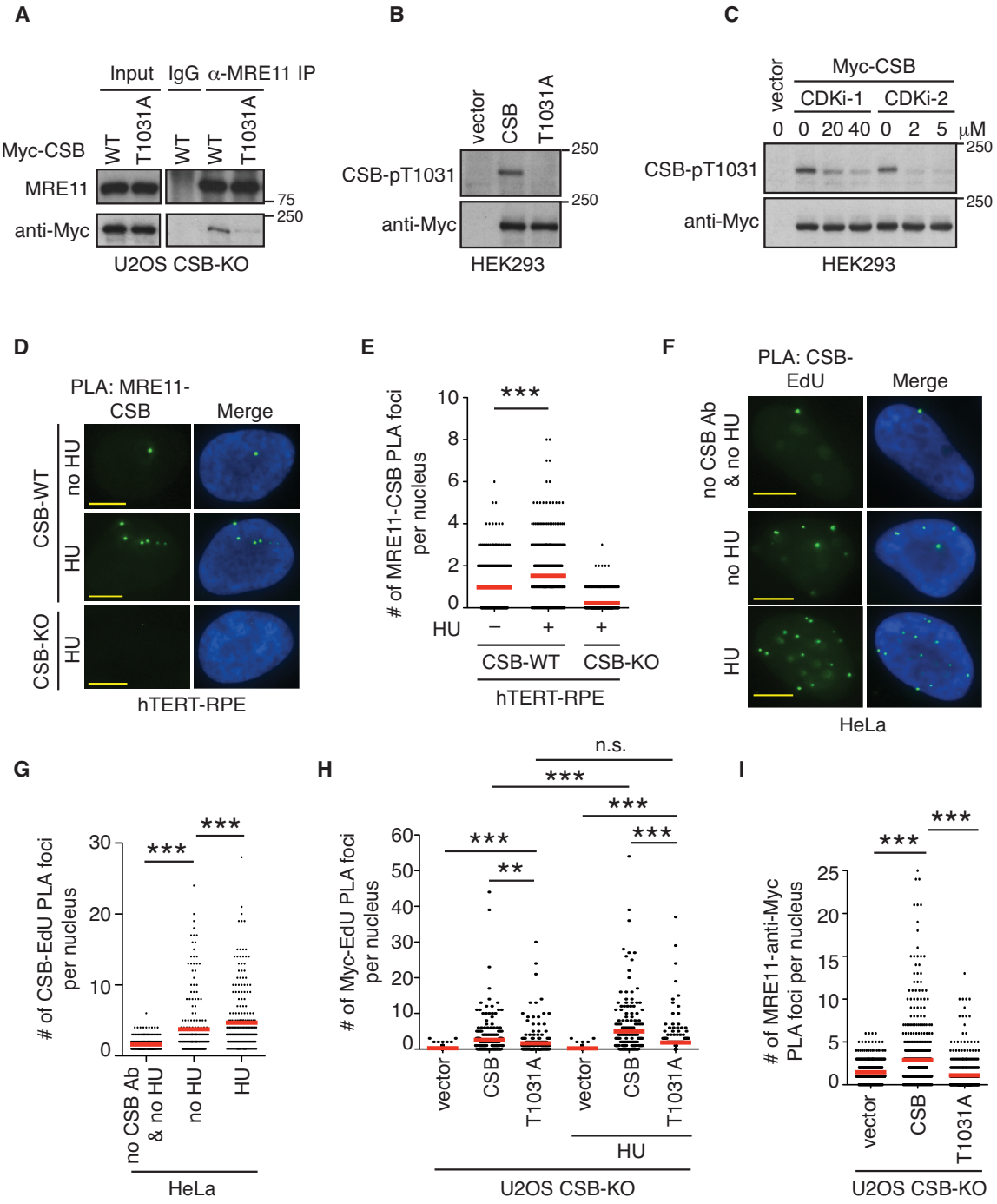

Figure 1. CDK-dependent CSB phosphorylation on T1031 mediates the CSB–MRE11 interaction at stalled forks. (**A**) Anti-MRE11 coIPs in U2OS CSB-KO cells stably expressing Myc-CSB WT or Myc-CSB-T1031A. Immunoblotting was performed with anti-MRE11 and anti-Myc antibodies. (**B**) Western analysis of HEK293 cells transfected with the vector alone, Myc-CSB or Myc-CSB-T1031A. Immunoblotting was performed with anti-CSB-pT1031 and anti-Myc antibodies. (**C**) Western analysis. HEK293 cells transfected with the vector alone or Myc-CSB were treated with no CDK inhibitor or varying doses of roscovitine (CDKi-1) or CGP74514A (CDKi-2). Immunoblotting was performed with anti-CSB-pT1031 and anti-Myc antibodies. (**D**) Representative images of PLA between MRE11 and CSB at ongoing (no HU) or stalled (HU) forks. hTERT-RPE CSB-WT and CSB-KO cells were treated with no HU or 4 mM HU, and fixed 4 h later. Nuclei were stained with DAPI in blue in this and subsequent panels. Scale bars in this and subsequent panels: 5 μm. (**E**) Quantification of PLA between MRE11 and CSB from panel (D). The respective numbers of cells analyzed for hTERT-RPE CSB-WT (−HU), hTERT-RPE CSB-WT (+HU) and hTERT-RPE CSB-KO (+HU) were 379, 360 and 365. Data from single experiments are represented as scatter plot graphs with the mean indicated in this panel and panels (G)–(I). The *P*-value was determined using a nonparametric Mann–Whitney rank-sum *t*-test in this panel and panels (G)–(I). ***$P < 0.001$. (**F**) Representative images of PLA between endogenous CSB and EdU in HeLa cells at ongoing (no HU) or stalled (HU) forks. No CSB antibody was included as a negative control. (**G**) Quantification of PLA between CSB and EdU from panel (F). The respective numbers of cells analyzed were 234 (no CSB Ab & no HU), 220 (no HU) and 231 (HU). ***$P < 0.001$. (**H**) Quantification of PLA between EdU and Myc-CSB alleles. A total of 218–249 cells per condition were analyzed. **$P < 0.01$; ***$P < 0.001$; n.s.: $P > 0.05$. (**I**) Quantification of PLA between MRE11 and Myc-CSB alleles. The respective numbers of cells analyzed for vector, Myc-CSB and Myc-CSB-T1031 (+HU) were 580, 589 and 594. ***$P < 0.001$.

results suggest that T1031 phosphorylation mediates recruitment of CSB to stalled forks. We noticed that in untreated U2OS CSB-KO cells, Myc-CSB-T1031A was able to form EdU PLA foci albeit at a reduced level compared to Myc-CSB (Figure 1H), indicating that T1031 phosphorylation is not essential for CSB's association with replication forks in unperturbed cells.

CSB is an ATP-dependent chromatin remodeler and we have previously reported that the ATPase-dead W851R mutation abrogates CSB's chromatin remodeling activity *in vivo* (27). Unlike the T1031A mutation, this ATPase-dead W851R mutation had little effect on the PLA foci formation between Myc-CSB and EdU in HU-treated U2OS CSB-KO cells (Supplementary Figure S2D). In addition, the W851R mutation did not affect the ability of Myc-CSB to interact with mCherry-LacR-MRE11 at the lac operator array in U2OS-265 CSB-KO cells (Supplementary Figure S2E). These results suggest that the ATPase activity of CSB is dispensable for both its association with stalled forks and its interaction with MRE11.

CSB promotes MRE11 recruitment to stalled forks in the absence of BRCA1/2 but not in wild-type cells

MRE11 is recruited to stalled forks and this recruitment is further stimulated in BRCA1/2-deficient cells (17,18). To investigate whether CSB regulates MRE11 recruitment to stalled forks, we first examined HU-induced MRE11 foci formation, a readout for MRE11 association with stalled forks, in both U2OS CSB-WT and CSB-KO cells that were transfected with siControl, siBRCA1 or siBRCA2 (Supplementary Figure S3A). We observed that loss of CSB did not affect HU-induced MRE11 foci formation in EdU+ U2OS cells (Figure 2A). While depletion of either BRCA1 or BRCA2 led to a further increase in the number of EdU+ cells with HU-induced MRE11 foci in U2OS CSB-WT cells, this further increase was not observed in U2OS CSB-KO cells depleted for either BRCA1 or BRCA2 (Figure 2A). This defect was also observed in U2OS CSB-KO cells in which BRCA1 or BRCA2 was depleted with a second independent siRNA (siBRCA1-2 or siBRCA2-2) (Figure 2B). To further substantiate this observation, we pulse labeled both U2OS CSB-WT and CSB-KO cells that were depleted with either BRCA1 or BRCA2 with EdU for 10 min prior to HU treatment. Analysis of PLA foci formation of MRE11 with EdU revealed that depletion of either BRCA1 or BRCA2 increased the MRE11–EdU PLA foci formation in HU-treated U2OS CSB-WT cells, but this increase was abolished in HU-treated U2OS CSB-KO cells (Figure 2C). Taken together, these results suggest that CSB does not regulate MRE11 recruitment to stalled forks in wild-type cells but promotes further MRE11 recruitment to stalled forks in BRCA1/2-deficient cells.

CSB's phosphorylation on T1031 but not CSB's ATPase activity mediates further MRE11 recruitment to stalled forks in BRCA1/2-deficient cells

To investigate whether CSB is dependent upon its T1031 phosphorylation or its ATPase activity to regulate MRE11 recruitment to stalled forks, we measured the MRE11–EdU PLA foci formation in BRCA1/2-depleted U2OS CSB-KO cells transfected with the vector alone, Myc-CSB, Myc-CSB-T1031A or Myc-CSB-W851R. We observed that the T1031A mutation abrogated the ability of Myc-CSB to restore MRE11–EdU PLA foci formation in BRCA2-depleted U2OS CSB-KO cells (Figure 2D). In agreement with this finding, the T1031A mutation also abolished the ability of Myc-CSB to restore HU-induced MRE11 foci formation in BRCA1/2-depleted U2OS CSB-KO cells (Figure 2E). Furthermore, treatment with CDK inhibitor CGP74514A (CDKi-2) abrogated the ability of Myc-CSB to restore HU-induced MRE11 foci formation in BRCA1/2-depleted U2OS CSB-KO cells (Figure 2F). Altogether, these results suggest that CDK-dependent phosphorylation of CSB on T1031 is necessary to promote further MRE11 recruitment to stalled forks in BRCA1/2-deficient cells.

We observed that unlike Myc-CSB-T1031A, Myc-CSB-W851R behaved like Myc-CSB in supporting MRE11–EdU PLA foci formation as well as HU-induced MRE11 foci formation (Figure 2D and G). These results suggest that CSB does not require its ATPase activity to promote further MRE11 recruitment to stalled forks in BRCA1/2-deficient cells.

CSB promotes fork degradation in BRCA1- or BRCA2-depleted cells in a manner dependent upon both its T1031 phosphorylation and its ATPase activity

MRE11 degrades nascent DNA strands at reversed forks, which is blocked by BRCA1 and BRCA2 (16–19). Nascent DNA strands can also be degraded by DNA2, which is prohibited by CtIP and BOD1L (54,55). To investigate whether CSB interacts with MRE11 to regulate fork stability in BRCA1- or BRCA2-deficient cells, we depleted BRCA1 or BRCA2 in three different cell types (U2OS, HCT116 and hTERT-RPE) that were either wild type for CSB (CSB-WT) or knocked out for CSB (CSB-KO) (Supplementary Figure S3A). These cells were first labeled with IdU for 20 min and then with CldU for 20 min prior to treatment with HU for 5 h (top panel in Figure 3A and Supplementary Figure S3B). DNA fiber analysis revealed that knockdown of BRCA1 or BRCA2 led to a significant reduction in the ratio of CldU/IdU in U2OS, HCT116 or hTERT-RPE cells (Figure 3A and B, and Supplementary Figure S3B and C), in agreement with previous reports (17,18). Loss of CSB reversed this reduction in the ratio of CldU/IdU in BRCA1- or BRCA2-depleted U2OS, HCT116 or hTERT-RPE cells (Figure 3A and B, and Supplementary Figure S3B and C). The effect of loss of CSB on restoring fork protection in BRCA2-depleted cells was similar to that of MRE11 inhibition (Figure 3C). Loss of CSB was also observed to reverse the reduction in the ratio of CIdU/IdU in U2OS cells that were depleted with a second siRNA against BRCA1 (siBRCA1-2) or BRCA2 (siBRCA2-2) (Supplementary Figure S3D). It has been reported that HU, but not the DNA polymerase inhibitor aphidicolin, induces metabolic reactive oxygen species (56). We observed that loss of CSB also prevented fork degradation in aphidicolin-treated BRCA1/2-depleted cells (Supplementary Figure S3E), suggesting that the role of CSB in promoting fork degradation in BRCA1/2-deficient cells

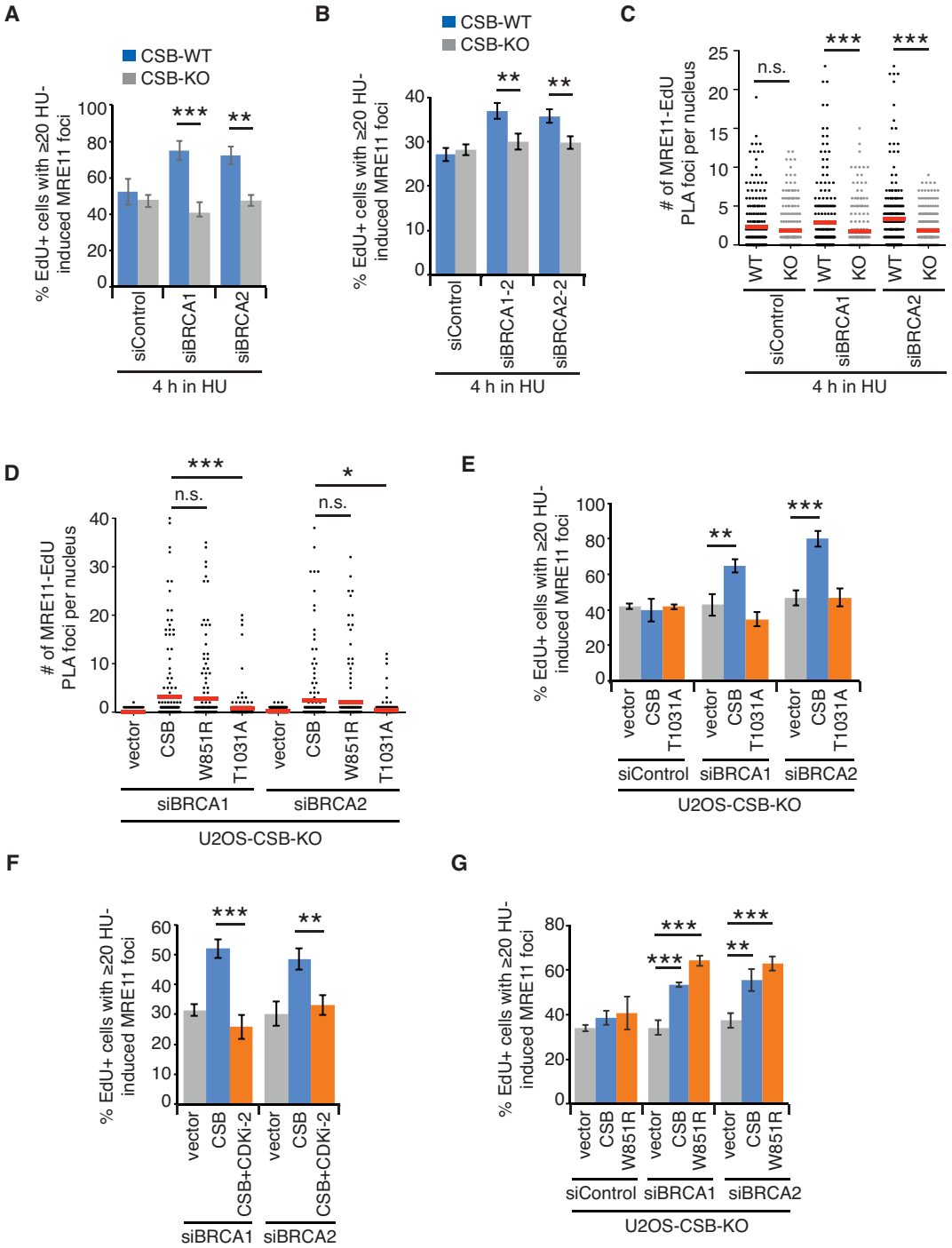

Figure 2. CSB promotes MRE11 recruitment to stalled forks in BRCA1/2-depleted cells but not in wild-type cells. (**A**) Quantification of the percentage of EdU+ cells with ≥20 HU-induced MRE11 foci. U2OS CSB-WT and CSB-KO cells were transfected with siControl, siBRCA1 or siBRCA2 for 48 h, and then incubated with EdU for 10 min, followed by treatment with HU for 4 h. A total of 500–550 cells per condition were scored in a blind manner. Standard deviations from three independent experiments are indicated in this panel and panels (B) and (E)–(G). $^{**}P < 0.01$; $^{***}P < 0.001$. (**B**) Quantification of the percentage of EdU+ cells with ≥20 HU-induced MRE11 foci. U2OS CSB-WT and CSB-KO cells were transfected with siControl, or a second set of siRNA against BRCA1 (siBRCA1-2) or BRCA2 (siBRCA2-2). Scoring was done as in panel (A). (**C**) Quantification of PLA foci between MRE11 and EdU in both U2OS CSB-WT and CSB-KO cells transfected with siControl, siBRCA1 or siBRCA2. A total of 187–212 cells per condition were analyzed. $^{*}P < 0.05$; $^{***}P < 0.001$; n.s.: $P > 0.05$. (**D**) Quantification of PLA foci between MRE11 and EdU in siBRCA1/2-depleted CSB-KO cells expressing the vector alone, Myc-CSB, Myc-CSB-W851R or Myc-CSB-T1031A. A total of 173–217 cells per condition were analyzed. $^{*}P < 0.05$; $^{***}P < 0.001$; n.s.: $P > 0.05$. (**E**) Quantification of the percentage of EdU+ cells as indicated with ≥20 HU-induced MRE11 foci. Scoring was done as in panel (A). $^{**}P < 0.01$; $^{***}P < 0.001$. (**F**) Quantification of the percentage of EdU+ cells with ≥20 HU-induced MRE11 foci. BRCA1/2-depleted U2OS CSB-KO cells transfected with the vector alone or Myc-CSB were incubated with EdU for 10 min, followed by treatment with HU for 4 h in the presence or absence of 2 μM CDKi-2 inhibitor. Scoring was done as in panel (A). $^{**}P < 0.01$; $^{***}P < 0.001$. (**G**) Quantification of the percentage of EdU+ cells as indicated with ≥20 HU-induced MRE11 foci. Scoring was done as in panel (A). $^{**}P < 0.01$; $^{***}P < 0.001$.

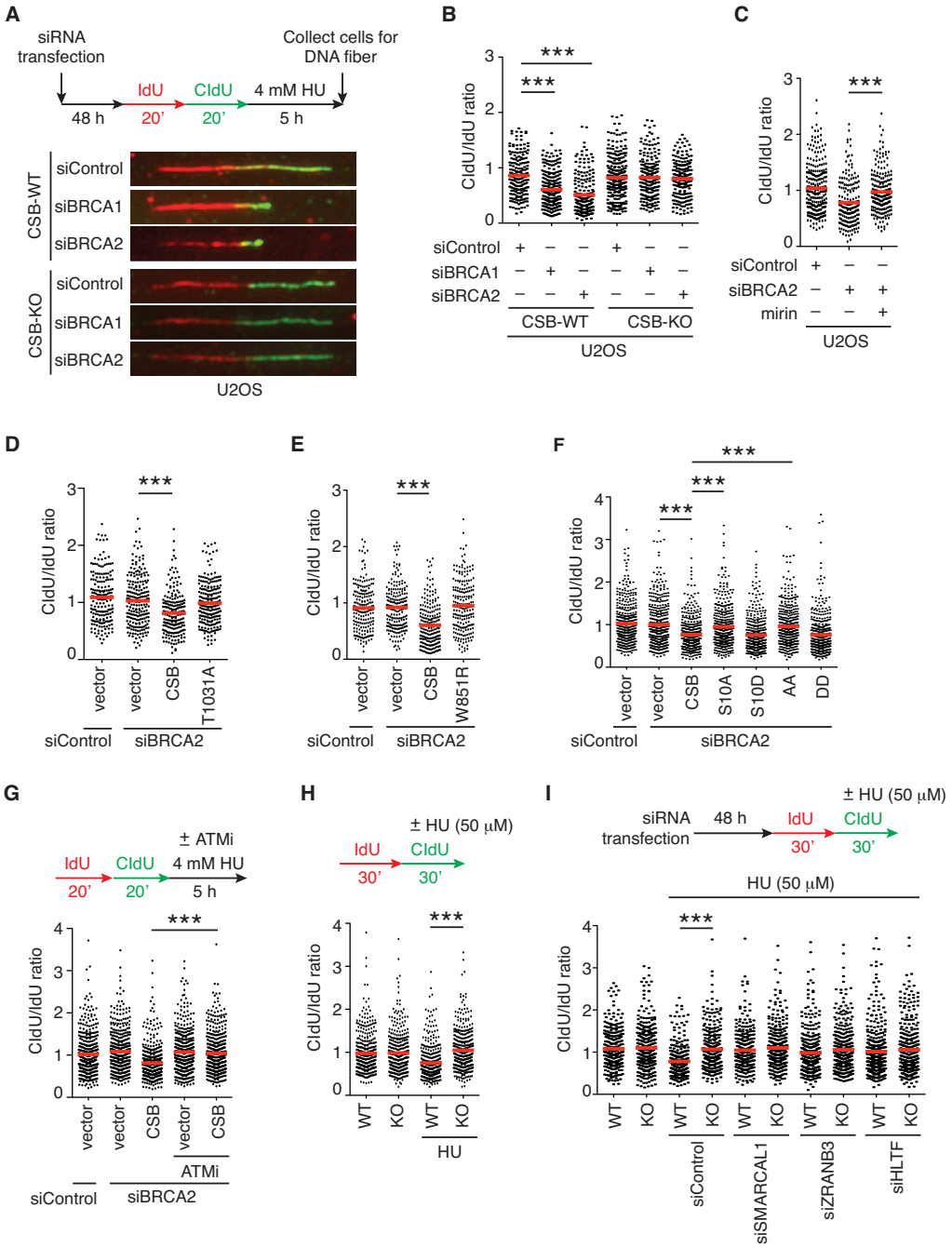

Figure 3. CSB promotes MRE11-mediated degradation of nascent DNA strands in BRCA1/2-depleted cells. (**A**) Representative images of DNA fibers from U2OS CSB-WT or CSB-KO. Following transfection with indicated siRNA, cells were incubated first with IdU (red) and then with CldU (green), followed by treatment with 4 mM HU for 5 h. (**B**) Quantification of the CldU/IdU ratio. A total of 193–274 fibers per condition were analyzed. Data from single experiments are represented as scatter plot graphs with the mean indicated in this and subsequent panels. The *P*-value was determined using a nonparametric Mann–Whitney rank-sum *t*-test in this and subsequent panels. ***$P < 0.001$. (**C**) Quantification of the CldU/IdU ratio for BRCA2-depleted U2OS cells. Following incubation with CldU (green), cells were treated with HU as in panel (A) in the presence or absence of 50 μM mirin. A total of 190–251 fibers per condition were analyzed. ***$P < 0.001$. (**D**) Quantification of the CldU/IdU ratio for BRCA2-depleted U2OS CSB-KO cells complemented with the vector alone, Myc-CSB or Myc-CSB-T1031A. A total of 201–233 fibers per condition were analyzed. ***$P < 0.001$. (**E**) Quantification of the CldU/IdU ratio for BRCA2-depleted U2OS CSB-KO cells transfected with the vector alone, Myc-CSB or Myc-CSB-W851R. A total of 202–218 fibers per condition were scored. ***$P < 0.001$. (**F**) Quantification of the CldU/IdU ratio for BRCA2-depleted U2OS CSB-KO cells transfected with the vector alone, Myc-CSB, Myc-CSB-S10A, Myc-CSB-S10D, Myc-CSB-S10A-S158A (CSB-AA) or Myc-CSB-S10D-S158D (CSB-DD). A total of 411–424 fibers per condition were scored. ***$P < 0.001$. (**G**) Quantification of the CldU/IdU ratio for BRCA2-depleted U2OS cells expressing the vector alone or Myc-CSB. Following incubation with CldU (green), cells were treated with HU as in panel (A) in the presence or absence of 10 μM ATM inhibitor KU55933. A total of 412–434 fibers per condition were analyzed. ***$P < 0.001$. (**H**) Quantification of the CldU/IdU ratio for both U2OS CSB-WT and CSB-KO cells. Cells were incubated with CldU (green) in the presence or absence of 50 μM HU. A total of 362–382 fibers per condition were analyzed. ***$P < 0.001$. (**I**) Quantification of the CldU/IdU ratio for both U2OS CSB-WT and CSB-KO cells transfected with siControl, siSMARCAL1, siZRANB3 or siHLTF. A total of 279–364 fibers per condition were analyzed. ***$P < 0.001$.

is not limited to only HU-induced stalled forks. In contrast, loss of CSB did not reverse fork degradation in CtIP- and BOD1L-depleted U2OS cells (Supplementary Figure S4A–C). These results suggest that CSB promotes MRE11-mediated fork degradation in BRCA1/2-deficient cells.

Further DNA fiber analysis revealed that while overexpression of Myc-CSB promoted fork degradation in BRCA2-depleted CSB-KO cells, overexpression of either Myc-CSB-T1031A or Myc-CSB-W851R failed to do so in two independent experiments (Figure 3D and E, and Supplementary Figure S3F), suggesting that CSB is dependent upon both its T1031 phosphorylation and its ATPase activity to promote MRE11-dependent fork degradation in BRCA2-deficient cells.

We have previously reported that phosphorylation of CSB on S10 by ATM controls ATP-dependent chromatin remodeling activity of CSB at DSBs (27). To investigate whether CSB phosphorylation on S10 is required for fork degradation, we transfected BRCA2-depleted U2OS CSB-KO cells with the vector alone, Myc-CSB, Myc-CSB carrying a nonphosphorylatable S10A mutation (Myc-CSB-S10A) or Myc-CSB carrying a phosphomimetic S10D mutation (Myc-CSB-S10D). We observed that overexpression of Myc-CSB-S10A was unable to restore the reduction in the ratio of CldU/IdU in BRCA2-depleted U2OS CSB-KO cells, whereas overexpression of Myc-CSB-S10D was fully competent in doing so, indistinguishable from overexpression of Myc-CSB (Figure 3F). In addition, treatment with ATM inhibitor KU55933 abrogated the ability of Myc-CSB to restore the reduction in the ratio of CldU/IdU in BRCA2-depleted U2OS CSB-KO cells (Figure 3G). These results suggest that ATM controls the ATP-dependent activity of CSB that is necessary to promote fork degradation in BRCA1/2-deficient cells.

CSB regulates slowdown in fork progression in the presence of mild replication stress

Fork reversal has been reported to be a prerequisite for MRE11-dependent fork degradation in BRCA1/2-deficient cells (6,7,14). Our finding that CSB, a DNA translocase, promotes MRE11-dependent fork degradation in BRCA1/2-depleted cells prompted us to ask whether CSB regulates fork reversal. It has been reported that fork reversal impedes fork progression in the presence of a low level of replication stress (9) and that depletion of fork reversal proteins such as HLTF and ZRANB3 prevents fork slowing (11,57). To investigate whether CSB regulates fork reversal to promote fork slowing, we treated both U2OS CSB-WT and CSB-KO cells with a low dose of HU (50 μM), which has been reported to induce fork reversal and slows down fork progression (57). We first labeled cells with IdU for 30 min and then with CldU for 30 min in the presence of 50 μM HU. In agreement with previous findings, this low dose of HU slowed down fork progression in U2OS CSB-WT cells as evidenced by a reduction in the ratio of CIdU/IdU (Figure 3H). This reduction was reversed in U2OS CSB-KO cells (Figure 3H), indicating that CSB plays a role in regulating fork reversal *in vivo*.

To investigate whether CSB functions with fork reversal proteins such as SMARCAL, ZRANB3 or HLTF to regulate fork progression, we depleted these proteins individually in both U2OS CSB-WT and CSB-KO cells. DNA fiber analysis revealed that depletion of SMARCAL1, ZRANB3 or HLTF prevented slowdown in fork regression in U2OS CSB-WT cells exposed to 50 μM HU (Figure 3I), in agreement with previous findings (9,11,57). Depletion of SMARCAL1, ZRANB3 or HLTF did not lead to any further increase in fork progression in U2OS CSB-KO cells exposed to 50 μM HU (Figure 3I). These results suggest that CSB regulates fork slowing upon exposure to replication stress in a manner similar to SMARCAL1, ZRANB3 and HLTF.

CSB exhibits an intrinsic ATP-dependent fork reversal activity that is inhibited by its N-terminal region

To investigate whether CSB catalyzes fork reversal *in vitro*, we produced baculovirus-expressed recombinant CSB full-length protein (Figure 4A) and examined its activity using a previously reported fork reversal assay (12). Recombinant CSB-WT showed little *in vitro* fork reversal activity (Figure 4B). It has been reported that the CSB N-terminal region autoinhibits its ATPase activity both *in vivo* and *in vitro* (26,27). Therefore, we investigated whether deleting the N-terminal region might enable CSB to catalyze fork reversal *in vitro*. We produced three baculovirus-expressed recombinant CSB truncation mutants lacking varying lengths of the N-terminal region (CSB-230, CSB-360 and CSB-447) (Figure 4A). Interestingly, all three CSB truncation mutants exhibited fork reversal activity in a manner dependent upon the presence of ATP (Figure 4B and C). To further substantiate that these CSB truncation mutants are dependent upon their ATPase activity to catalyze fork reversal *in vitro*, we produced recombinant CSB-360 mutant carrying the ATPase-dead W851R mutation (Figure 5A). Unlike the recombinant CSB-360 protein, the CSB-360-W851R protein was defective in catalyzing fork reversal *in vitro* (Figure 5B). Altogether, these results suggest that CSB possesses an intrinsic ATP-dependent fork reversal activity that is inhibited by its N-terminal region.

It has been reported that CSB phosphorylation on both S10 and S158 releases the autoinhibition of CSB's N-terminal region to promote its ATP-dependent chromatin remodeling *in vivo* (27). Therefore, we asked whether CSB carrying double phosphomimetic S10D-S158D mutations might be enabled to catalyze fork reversal *in vitro*. We produced recombinant CSB-S10D-S158D mutant protein (Figure 5A); however, little fork reversal activity was observed with this CSB-S10D-S158D mutant (Figure 5B). In contrast, Myc-tagged CSB-S10D-S158D (CSB-DD) was fully competent in promoting fork degradation in BRCA2-depleted cells, whereas Myc-tagged CSB carrying double nonphosphorylatable S10A-S158A (CSB-AA) failed to do so (Figure 3F). These results altogether suggest that CSB phosphorylation on both S10 and S158 alone is insufficient to release the autoinhibition of the CSB N-terminal region for fork reversal activity *in vitro*.

To gain further insight into the fork reversal activity of the CSB-360 protein, we tested its activity on additional DNA substrates, including dsDNA, G4 DNA and forked substrates with ssDNA on both tails or ssDNA on one tail. The CSB-360 protein did not exhibit any DNA unwinding

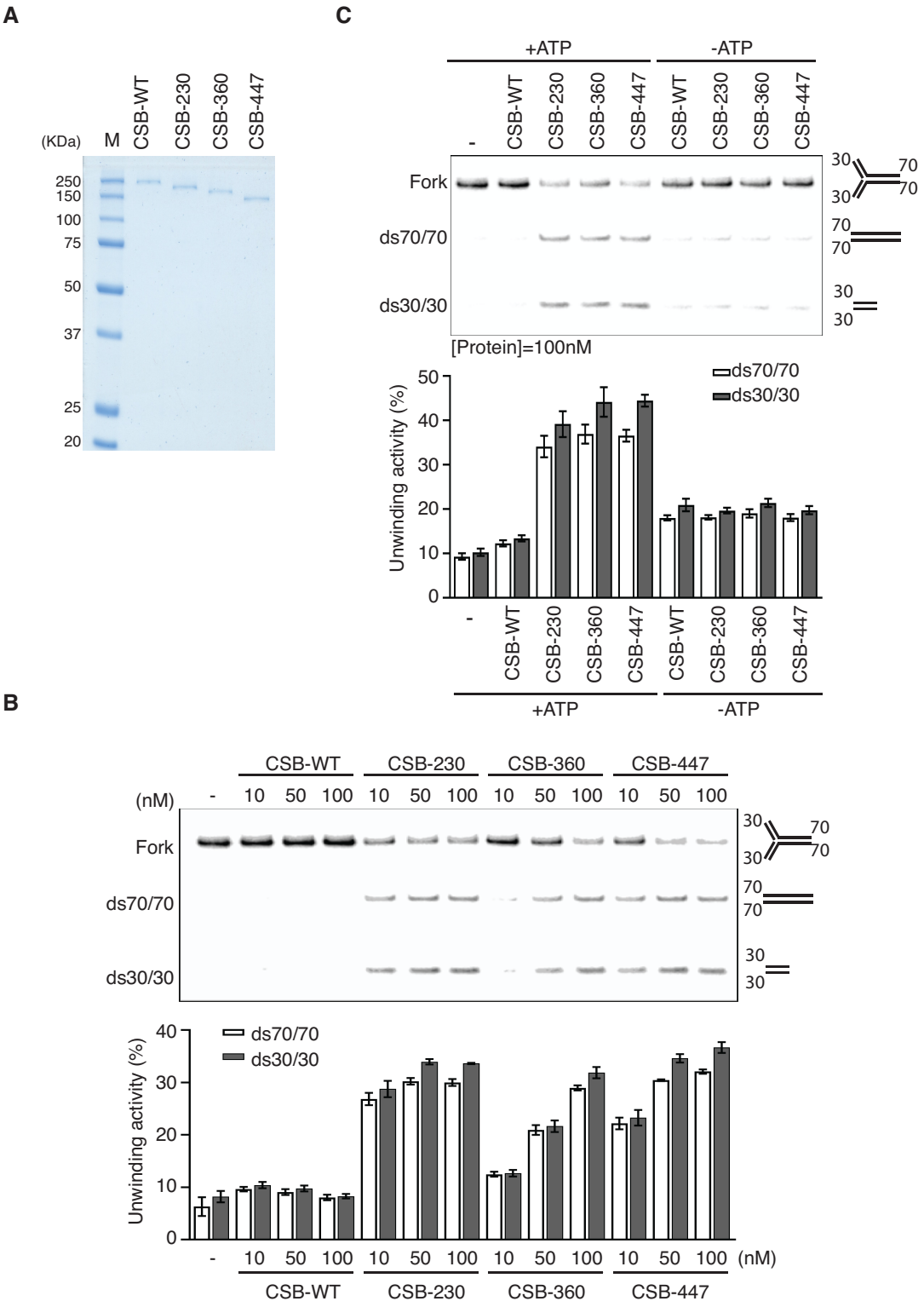

Figure 4. CSB possesses *in vitro* fork reversal activity that is inhibited by its N-terminal region. (**A**) Coomassie staining of purified CSB-WT, CSB-230, CSB-360, and CSB-447 truncation mutants purified from Sf9 insect cells. (**B**) Fork reversal assays in the presence of increasing concentration (10, 50 and 100 nM) of the indicated CSB proteins (top panel). The bottom panel represents the quantifications obtained from the upper panel. The mean and standard deviations are representative of three independent experiments. (**C**) Fork reversal assays in the presence or absence of ATP and the indicated purified CSB proteins (top panel). The bottom panel represents the quantifications obtained from the upper panel in three independent experiments.

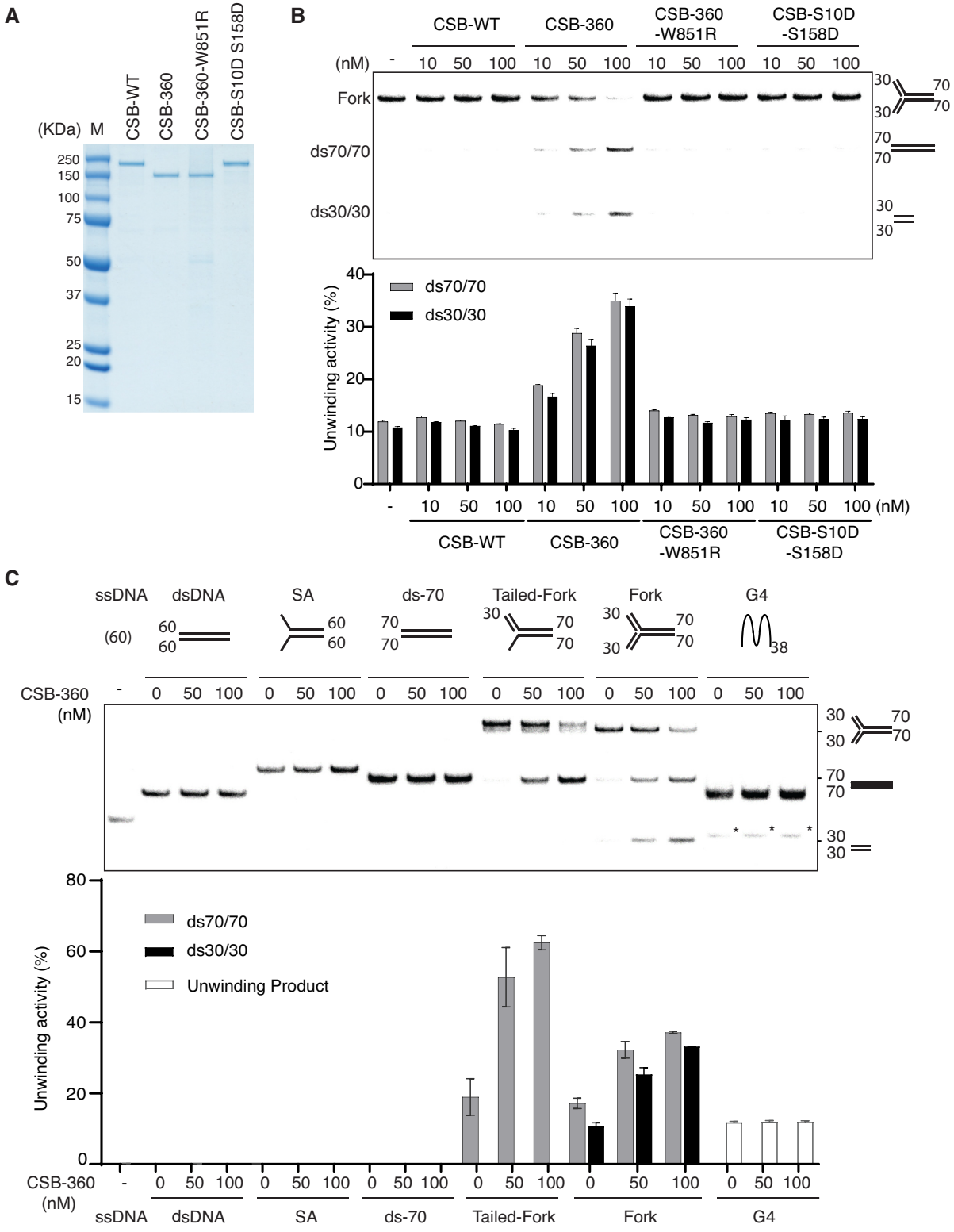

Figure 5. CSB-360 requires its ATPase activity to catalyze fork reversal. (**A**) Coomassie staining of purified wild-type CSB, CSB-360, CSB-360-W851R and CSB-S10D-S158D purified from Sf9 insect cells. (**B**) Fork reversal assays with an increasing concentration (10, 50 and 100 nM) of CSB-WT, CSB-360, CSB-360-W851R and CSB-S10D-S158D as indicated (top panel). The bottom panel represents the quantifications obtained from the upper panel in three independent experiments. (**C**) Fork reversal assays with various DNA substrates and an increasing concentration of CSB-360 (50 and 100 nM) as indicated (top panel). An asterisk indicates nonspecific denaturation of the structured G4 probe in the reaction buffer. The bottom panel represents the quantifications obtained from the upper panel in three independent experiments.

activity on 60-bp dsDNA, G4 DNA or the forked DNA substrate with ssDNA on both tails (Figure 5C), in agreement with previous reports that CSB does not unwind dsDNA (58,59) nor G4 DNA in the absence of cDNA (60). On the other hand, the CSB-360 protein exhibited fork reversal activity on the forked DNA substrate with ssDNA on one tail and this activity was higher than that of the CSB-360 protein on the forked substrate with no ssDNA on both tails (Figure 5C), indicating that the CSB-360 protein may have a preference for certain forked substrates. Taken together, these results suggest that it is unlikely that CSB-360 protein unwinds DNA to catalyze fork reversal, but rather is more likely to utilize its translocase activity for this function.

CSB acts in the same pathway as MRE11 to promote restart of stalled forks

In addition to fork stability and fork progression, we also investigated whether CSB regulates the restart of stalled forks. We performed DNA fiber analysis using three different cell lines (U2OS, HCT116 and hTERT-RPE) that are either CSB-WT or CSB-KO. These cells were first labeled with IdU for 20 min, treated with HU for 4 h and then labeled with CldU for 60 min. Loss of CSB did not affect the number of newly fired origins (Figure 6A and B, and Supplementary Figure S5A and B). On the other hand, loss of CSB led to not only a decrease in the number of restarted forks but also an increase in the number of stalled forks in all three cell types examined (Figure 6A and B, and Supplementary Figure S5A and B), suggesting that CSB promotes restart of stalled forks.

Further DNA fiber analysis revealed that overexpression of Myc-CSB suppressed the number of stalled forks in U2OS CSB-KO cells, whereas overexpression of Myc-CSB-W851R failed to do so (Figure 6C), suggesting that CSB is dependent upon its ATPase activity to promote fork restart. In support of the notion that ATM controls CSB's ATPase activity at stalled forks, overexpression of Myc-CSB-S10D suppressed the number of stalled forks in U2OS CSB-KO cells, whereas overexpression of Myc-CSB-S10A failed to do so (Figure 6D). In contrast, overexpression of Myc-CSB-T1031A was fully competent in suppressing the number of stalled forks in U2OS CSB-KO cells (Figure 6C), suggesting that CSB phosphorylation on T1031 is dispensable for fork restart. These results further suggest that the T1031A mutation is a separation of function mutation and that CSB-mediated fork restart is mechanistically separable from CSB-mediated fork degradation in BRCA1/2-deficient cells.

Although CSB was not dependent upon its interaction with MRE11 to regulate fork restart, CSB was epistatic to MRE11 in regulating fork restart since treatment with MRE11 inhibitor mirin did not further increase the number of stalled forks in U2OS CSB-KO cells (Figure 6E). Treatment with mirin induced stalled forks in U2OS CSB-WT cells (Figure 6E), in agreement with previous findings (19). It has been suggested that MRE11 promotes fork restart through recombination-mediated processes such as HR and BIR (61–63). We have previously reported that CSB promotes BRCA1-mediated HR repair of DSBs (30). However, depletion of either BRCA1 or BRCA2 had little effect on the number of stalled forks in both U2OS CSB-WT and CSB-KO cells (Figure 6F), in agreement with previous reports that BRCA1/2-deficient cells exhibit no defect in replication recovery (17,18). These results suggest that CSB can promote fork restart independently of BRCA1/2-mediated HR.

CSB regulates BIR repair of DSBs

CSB has been previously reported to regulate a RAD52-dependent BIR pathway to repair ROS-induced DSBs (31). To investigate the role of CSB in BIR, we employed a previously published BIR reporter plasmid (pBIR-GFP) (24), in which restoration of GFP expression requires BIR repair of an I-SceI-induced DSB in the GFP gene. We found that loss of CSB led to a 31% reduction in BIR-dependent restoration of GFP expression in U2OS cells (Figure 6G), supporting the notion that CSB regulates BIR repair of DSBs. It has been reported that inactivation of BRCA1 reduces BIR efficiency (64). In agreement with the previous finding, depletion of BRCA1 impaired BIR-dependent restoration of GFP expression in U2OS CSB-WT cells (Figure 6H). Depletion of BRCA1 also led to a further decline in BIR-mediated restoration of GFP expression in U2OS CSB-KO cells (Figure 6H), suggesting that CSB is not epistatic to BRCA1 in regulating BIR.

CSB acts in the same pathway as RAD52 to prevent excessive replication stress-induced chromatid breaks in BRCA1/2-depleted cells

To investigate whether CSB regulates genomic stability in BRCA1/2-deficient cells exposed to replication stress, we examined chromosome abnormalities in BRCA1/2-depleted U2OS CSB-WT and CSB-KO cells following treatment with HU, olaparib or cisplatin. Analysis of metaphase chromosome spreads revealed that depletion of either BRCA1 or BRCA2 led to an accumulation of chromosome breaks and radial chromosomes in U2OS CSB-WT cells upon replication stress (Figure 7A and Supplementary Figure S6A–D), in agreement with previous reports (16–18). We noted that the effect of HU on radial chromosome formation was limited. A small increase in the accumulation of radial chromosomes was observed for BRCA1-depleted U2OS CSB-WT cells upon treatment with HU, whereas no radial chromosome accumulation was detected in BRCA2-depleted U2OS CSB-WT cells upon treatment with HU (Supplementary Figure S6D), suggesting that HU is a poor inducer of radial chromosomes in BRCA1/2-depleted CSB-WT cells under our experimental conditions.

We observed that loss of CSB in BRCA1/2-depleted U2OS cells promoted a further increase in the accumulation of chromatid breaks upon treatment with HU, olaparib or cisplatin (Figure 7A). In contrast, loss of CSB reduced the accumulation of radial chromosomes in BRCA1/2-depleted U2OS cells following treatment with HU, olaparib or cisplatin (Supplementary Figure S6D). It has been reported that ligase IV mediates radial chromosome formation in BRCA1/2-deficient cells (65). Perhaps, replication

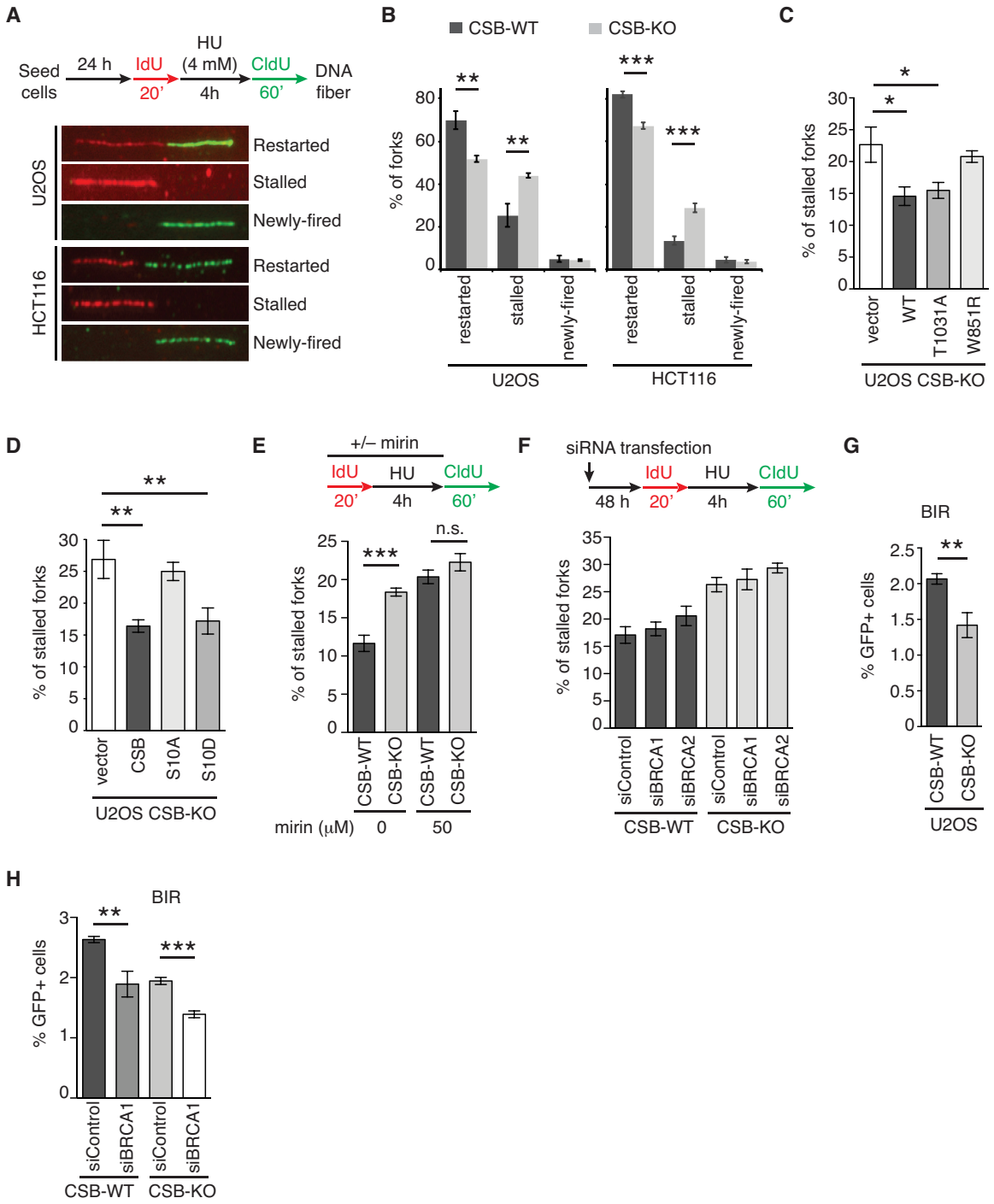

Figure 6. CSB promotes BIR-mediated fork restart. (**A**) Representative images of DNA fibers from U2OS and HCT116 cells that were first labeled with IdU (red), treated with HU and then labeled with CldU (green). (**B**) Quantification of the percentage of restarted, stalled or newly fired forks from U2OS and HCT116 that were either CSB-WT or CSB-KO. For U2OS CSB-WT and CSB-KO cells, a total of 423–456 fibers per condition for U2OS were scored in a blind manner. For HCT116 CSB-WT or CSB-KO cells, a total of 303–362 fibers per condition were scored in a blind manner. Standard deviations from three independent experiments are indicated in this and subsequent panels. $^{**}P < 0.01$; $^{***}P < 0.001$. (**C**) Quantification of the percentage of stalled forks in U2OS CSB-KO cells transfected with the vector alone, Myc-CSB WT, Myc-CSB-W851R or Myc-T1031A. A total of 318–386 fibers per condition were scored in a blind manner. $^{*}P < 0.05$. (**D**) Quantification of the percentage of stalled forks in U2OS CSB-KO cells transfected with the vector alone, Myc-CSB WT, Myc-CSB-S10A or Myc-CSB-S10D. A total of 523–577 fibers per condition were scored in a blind manner. $^{**}P < 0.01$. (**E**) Quantification of the percentage of stalled forks in U2OS CSB-WT and CSB-KO cells treated with or without 50 μM mirin. A total of 402–453 fibers per condition were scored in a blind manner. $^{***}P < 0.001$; n.s.: $P > 0.05$. (**F**) Quantification of the percentage of stalled forks in BRCA1/2-depleted U2OS CSB-WT and CSB-KO cells. A total of 383–494 fibers per condition were scored in a blind manner. (**G**) Quantification of the percentage of U2OS CSB-WT and CSB-KO cells with the restoration of GFP expression following BIR-mediated repair of I-SceI-induced DSBs. $^{**}P < 0.01$. (**H**) Quantification of the percentage of BRCA1-depleted U2OS CSB-WT and CSB-KO cells with the restoration of GFP expression following BIR-mediated repair of I-SceI-induced DSBs. $^{**}P < 0.01$; $^{***}P < 0.001$.

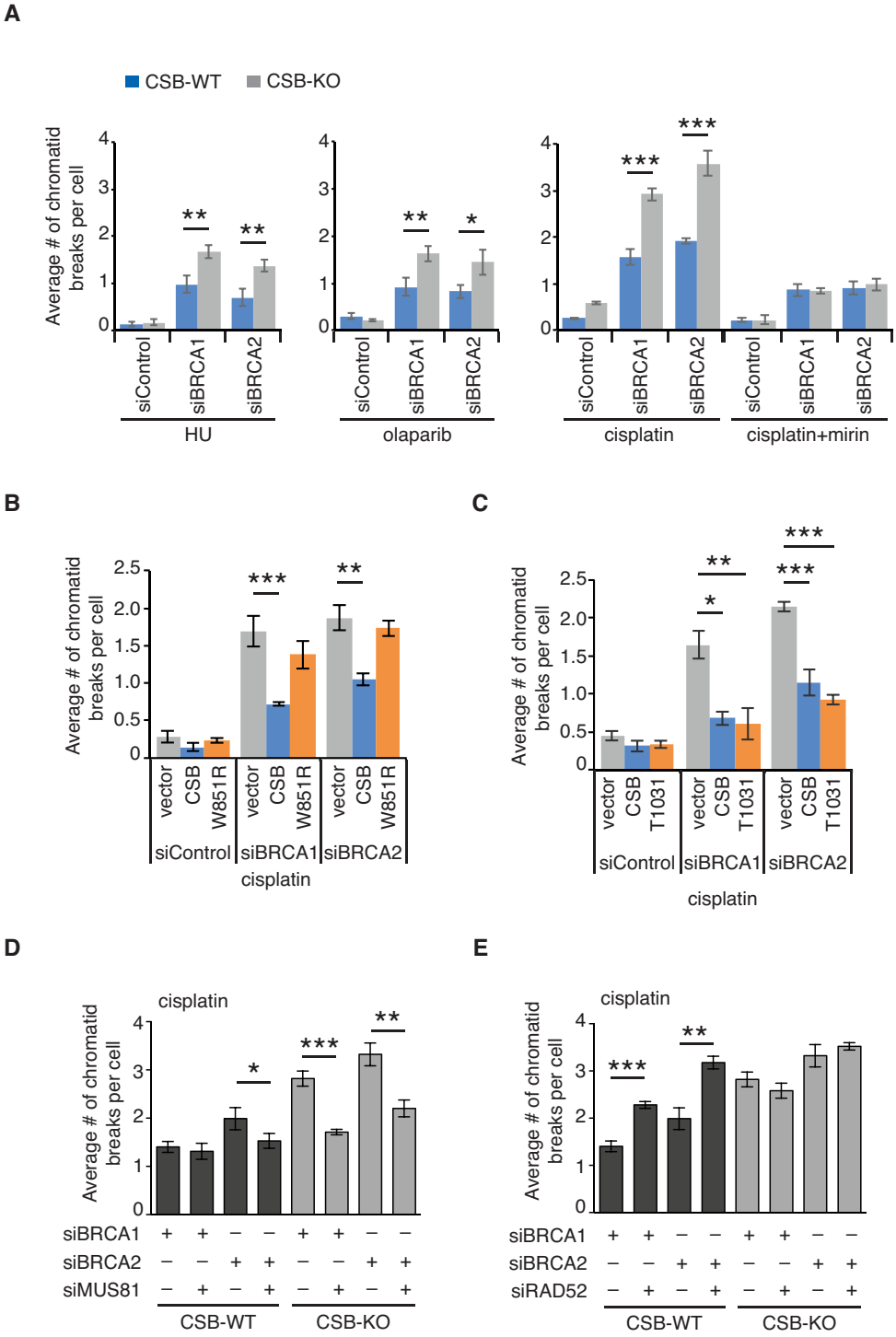

Figure 7. CSB acts epistatically with RAD52 to limit the excessive accumulation of replication stress-induced chromosome breaks in BRCA1/2-depleted cells. (**A**) Quantification of the average number of chromatin breaks per metaphase cell. U2OS CSB-WT and CSB-KO cells were transfected with indicated siRNA for 48 h. At least 20 metaphase cells per condition were scored in a blind manner. Standard deviations from three independent experiments are indicated in this and subsequent panels. $*P < 0.05$; $**P < 0.01$; $***P < 0.001$. (**B**) Quantification of the average number of chromatin breaks per cell. U2OS CSB-KO cells complemented with the vector alone, Myc-CSB or Myc-CSB-W851R were transfected with indicated siRNA prior to treatment with cisplatin for 5 h. Scoring was done as in panel (A). $**P < 0.01$; $***P < 0.001$. (**C**) Quantification of the average number of chromatin breaks per cell. U2OS CSB-KO cells complemented with the vector alone, Myc-CSB or Myc-CSB-T1031A were transfected with indicated siRNA prior to treatment with cisplatin for 5 h. Scoring was done as in panel (A). $*P < 0.05$; $**P < 0.01$; $***P < 0.001$. (**D**) Quantification of the average number of chromatin breaks per cell in cisplatin-treated U2OS CSB-WT and CSB-KO cells that were transfected with siMUS81 in combination with either siBRCA1 or siBRCA2. Scoring was done as in panel (A). $*P < 0.05$; $**P < 0.01$; $***P < 0.001$. (**E**) Quantification of the average number of chromatin breaks per cell in cisplatin-treated U2OS CSB-WT and CSB-KO cells that were transfected with siRAD52 in combination with either siBRCA1 or siBRCA2. Scoring was done as in panel (A). $**P < 0.01$; $***P < 0.001$.

stress-induced chromatid breaks accumulated in the absence of CSB are not compatible with ligase IV-mediated end joining. These results altogether suggest that replication stress leads to an excessive accumulation of chromosome breaks in BRCA1/2-deficient CSB-KO cells.

Further analysis revealed that reintroduction of Myc-CSB suppressed the excessive accumulation of cisplatin-induced chromatid breaks in BRCA1/2-depleted U2OS CSB-KO cells (Figure 7B), demonstrating that the observed excessive accumulation of replication stress-induced chromatid breaks is specific to CSB. Overexpression of Myc-CSB-T1031A but not Myc-CSB-W851R suppressed the excessive accumulation of cisplatin-induced chromatid breaks in BRCA1/2-depleted U2OS CSB-KO cells (Figure 7B and C). These results suggest that CSB is dependent upon its ATPase activity but not its T1031 phosphorylation to limit the excessive accumulation of chromosome breaks in BRCA1/2-deficient cells.

It has been reported that inhibition of MRE11 alleviates chromosome aberrations induced by replication stress in BRCA2-deficient cells (15). To further investigate the mechanism by which CSB prevents an excessive accumulation of chromatid breaks in BRCA1/2-depleted U2OS cells upon replication stress, we treated BRCA1/2-depleted U2OS CSB-WT and CSB-KO cells with mirin. In agreement with the previous finding (15), treatment with mirin mitigated cisplatin-induced accumulation of both chromatid breaks and radial chromosomes in BRCA1/2-depleted U2OS CSB-WT cells (Figure 7A and Supplementary Figure S6D). Treatment with mirin also eliminated the effect of loss of CSB on cisplatin-induced chromatid break formation in BRCA1/2-depleted U2OS CSB-KO cells (Figure 7A). We have shown that fork protection is restored in BRCA1/2-deficient CSB-KO cells. These results suggest that the excessive formation of cisplatin-induced chromatid breaks in BRCA1/2-depleted CSB-KO cells is unlikely to arise from MRE11-mediated degradation of nascent DNA strands at reversed forks but rather MRE11-mediated repair of stalled forks. These results further imply that CSB acts downstream of MRE11 to promote repair of stalled forks.

MUS81 is a structure-specific endonuclease known to cleave stalled forks into DSBs that are thought to initiate RAD52-dependent MiDAS or BIR-like pathways to promote restart of stalled forks (15,25,42,66). We observed that depletion of MUS81 reduced the accumulation of cisplatin-induced chromatid breaks in BRCA1/2-depleted U2OS CSB-KO cells (Figure 7D and Supplementary Figure S7A), suggesting that MUS81-mediated cleavage of stalled forks is an underlying cause of excessive formation of chromatid breaks in BRCA1/2-depleted CSB-KO cells. In addition, depletion of RAD52 did not further increase the accumulation of cisplatin-induced chromatid breaks in BRCA1/2-depleted U2OS CSB-KO cells (Figure 7E and Supplementary Figure S7B). Taken together, these results suggest that CSB acts epistatically with RAD52 to promote BIR repair of stalled forks in BRCA1/2-deficient cells, thereby limiting the excessive accumulation of chromosome breaks.

Loss of CSB and BRCA1/2 deficiency are a toxic combination to cell survival upon replication stress

To investigate whether CSB regulates survival of BRCA1/2-deficient cells upon replication stress, we performed clonogenic survival assays in HCT116 CSB-WT and CSB-KO cells transfected with siControl, siBRCA1 or siBRCA1 following treatment with HU. While depletion of BRCA1 with two independent siRNAs (siBRCA1 and siBRCA1-2) did not affect the sensitivity of HCT116 cells to HU (Figure 8A and Supplementary Figure S8A), depletion of BRCA2 with two independent siRNAs (siBRCA2 and siBRCA2-2) enhanced the sensitivity of HCT116 cells to HU (Figure 8B and Supplementary Figure S8B). This increased sensitivity was also observed in BRCA2-depleted U2OS cells (Supplementary Figure S8C), suggesting that it is not limited to one cell type. Although the loss of CSB had little effect on the sensitivity of siControl-transfected HCT116 cells to HU, it resulted in synthetic sensitivity to HU in HCT116 cells that were depleted with either siBRCA1 or siBRCA1-2 (Figure 8A and Supplementary Figure S8A). In addition, loss of CSB further sensitized both BRCA2-depleted HCT116 and BRCA2-depleted U2OS cells to HU (Figure 8B, and Supplementary Figure S8B and C). Furthermore, loss of CSB together with BRCA1/2 deficiency resulted in a synthetic increase in the sensitivity of both HCT116 and U2OS cells to replication stress-inducing agents olaparib and cisplatin (Figure 8A and B, and Supplementary Figure S8C). Taken together, these results suggest that loss of CSB is toxic to BRCA1/2-deficient cells upon replication stress. Interestingly, analysis of published METABRIC breast cancer data (67,68) from cBioPortal (69,70) revealed that BRCA1 mutation-carrying breast cancer patients with low CSB expression had significant better overall survival and relapse free time than BRCA1 mutation-carrying breast cancer patients with high CSB expression (Figure 8C and D), in line with the notion that loss of CSB enhances chemosensitivity of cancers carrying BRCA mutations, thereby improving patient survival.

Further analysis revealed that overexpression of either Myc-CSB or Myc-CSB-T1031A improved survival of BRCA2-depleted U2OS CSB-KO cells in response to treatment with either olaparib or cisplatin (Figure 8E and F), suggesting that CSB is not dependent upon its T1031 phosphorylation to promote chemoresistance in BRCA2-deficient cells.

We have shown that CSB promotes MUS81-RAD52-mediated BIR to prevent excessive cisplatin-induced chromatid break formation in BRCA1/2-depleted cells. We observed that depletion of MUS81 had little effect on the sensitivity of BRCA1-depleted HCT116 cells to cisplatin (Supplementary Figure S8D), in agreement with previous reports that depletion of MUS81 does not affect chemosensitivity in BRCA1-deficient cells (15,71). On the other hand, depletion of MUS81 improved the survival of BRCA2-depleted HCT116 cells in response to cisplatin (Supplementary Figure S8E), in line with the notion that CSB promotes survival of BRCA2-deficient cells upon replication stress by facilitating BIR repair of DSBs arising from MUS81-mediated cleavage of stalled forks.

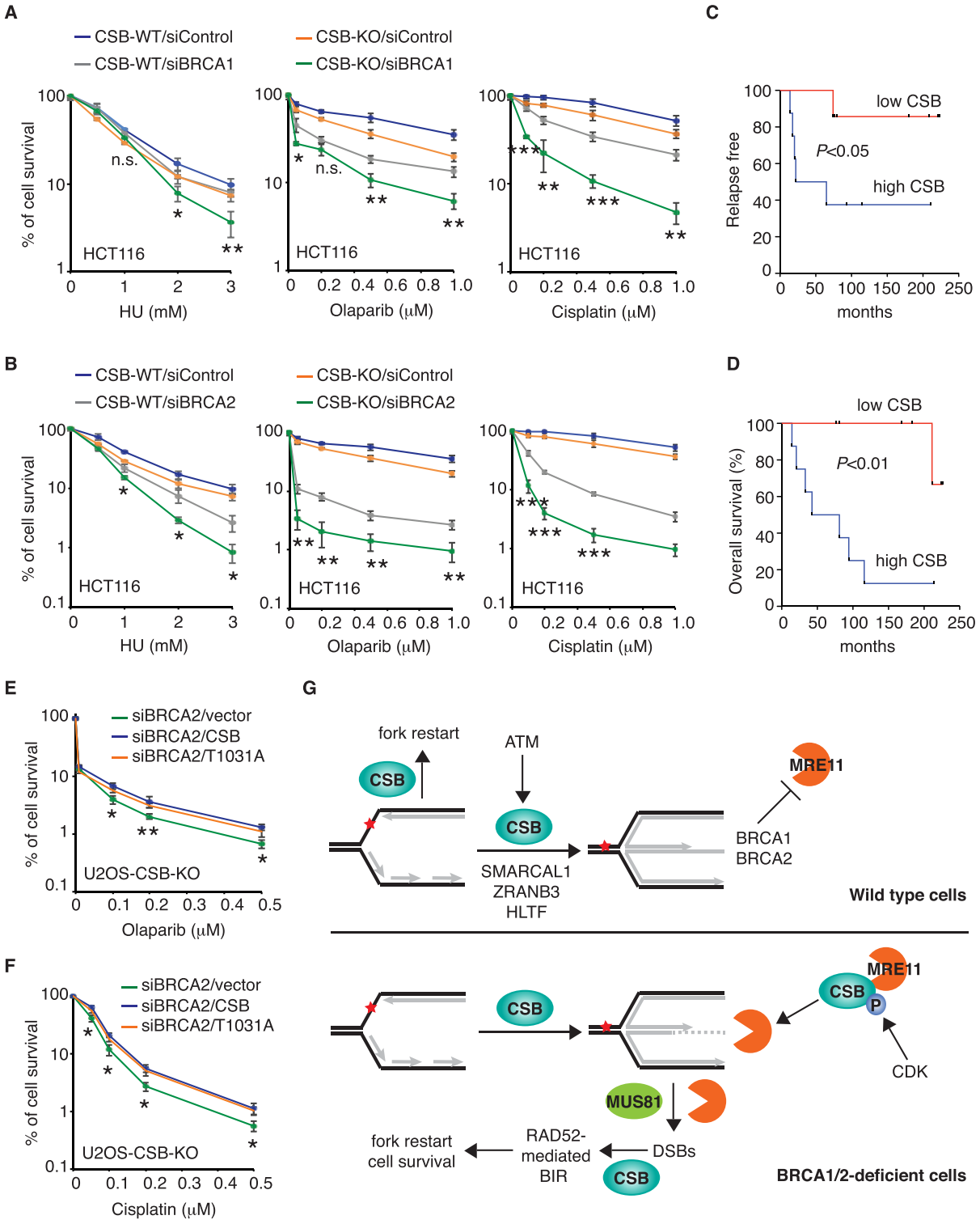

Figure 8. Loss of CSB is toxic to BRCA1/2-deficient cells exposed to replication stress. (**A**) Clonogenic survival assays of HCT116 CSB-WT and CSB-KO cells that were transfected with siControl or siBRCA1. Standard deviations from three independent experiments are indicated in this and subsequent panels. *P*-values for comparison between CSB-WT/siBRCA1 and CSB-KO/siBRCA1 are indicated. *$P < 0.05$; **$P < 0.01$; ***$P < 0.001$; n.s.: $P > 0.05$. (**B**) Clonogenic survival assays of both HCT116 CSB-WT and CSB-KO cells that were transfected with siControl or siBRCA2. *P*-values for comparison between CSB-WT/siBRCA2 and CSB-KO/siBRCA2 are indicated. *$P < 0.05$; **$P < 0.01$; ***$P < 0.001$; n.s.: $P > 0.05$. (**C**) Overall survival of BRCA1 mutation-bearing breast cancer patients with low or high CSB expression. Analysis was done on cBioPortal with METABRIC breast cancer data in this panel and panel (D). The *P*-value was derived using the log-rank (Mantel–Cox) test in this panel and panel (D). (**D**) Relapse free of BRCA1-bearing breast cancer patients with low or high CSB expression. Olaparib (**E**) and cisplatin (**F**) clonogenic survival assays of BRCA2-depleted U2OS CSB-KO cells that were complemented with the vector alone, Myc-CSB or Myc-CSB-T1031A. *P*-values for comparison between siBRCA2/vector and siBRCA2/T1031A are indicated. *$P < 0.05$; **$P < 0.01$. (**G**) Model for the function of CSB at stalled replication forks. See the text for details.

DISCUSSION

CSB is a DNA translocase and its ATPase activity has been reported to be stimulated by fork-like substrates (58). Several lines of evidence presented here suggest that CSB catalyzes fork reversal (Figure 8G). First, CSB possesses an intrinsic ATP-dependent fork reversal activity *in vitro*, albeit this activity is inhibited by its N-terminal region. It has been reported that the CSB's N-terminal region autoinhibits its ATPase activity both *in vivo* and *in vitro* (26,27). It is likely that CSB catalyzes fork reversal *in vivo* in a highly regulated manner. Second, it has been reported that fork reversal slows down fork progression (9,11,57), which can be prevented by depletion of known fork reversal factors such as SMARCAL1, ZRANB3 or HLTF (6,8,11,12). We have shown that loss of CSB prevents slowdown in fork progression in cells exposed to a low level of replication stress, which is similar to depletion of SMARCAL1, ZRANB3 or HLTF, indicative of a role of CSB in fork reversal *in vivo*. Third, it has been reported that fork reversal is a prerequisite for MRE11-dependent fork degradation in BRCA1/2-deficient cells (6,7,14). We have shown that CSB promotes MRE11-mediated fork degradation in BRCA1/2-deficient cells in a manner dependent upon its ATPase activity, in line with the notion that CSB catalyzes fork reversal. Our finding that ATM releases the autoinhibition of CSB's N-terminal region on CSB's ATPase activity needed for MRE11-dependent fork degradation *in vivo* suggests that ATM might control the fork reversal activity of CSB *in vivo*.

We have shown that CSB is recruited to stalled forks in a manner dependent upon CSB phosphorylation on T1031 by CDK. Our finding that T1031 phosphorylation mediates the CSB–MRE11 interaction suggests that CSB is likely recruited by MRE11 to stalled forks in wild-type cells, although we cannot rule out the possibility that CSB recruitment to stalled forks is independent from the CSB–MRE11 interaction. While dispensable for MRE11 association with stalled forks in wild-type cells, CSB is needed to promote elevated accumulation of MRE11 at stalled forks in BRCA1/2-deficient cells. One possibility could be that once recruited to stalled forks, CSB can in turn recruit MRE11 to stalled forks under pathological conditions lacking functional BRCA1/2 (Figure 8G). This is supported by our finding that the further accumulation of MRE11 at stalled forks in BRCA1/2-deficient cells is dependent upon T1031 phosphorylation, which mediates the CSB–MRE11 interaction. Another possibility could be that CSB remodels stalled forks, e.g. by promoting fork reversal, creating substrates favoring further association of MRE11 with stalled forks in the absence of BRCA1/2. However, this is not supported by our finding that the ATPase-dead CSB-W851R mutant, which cannot catalyze fork reversal, is fully competent to promote further accumulation of MRE11 at stalled forks in BRCA1/2-deficient cells. Our finding suggests that CSB uses distinctive mechanisms to regulate fork reversal and MRE11 recruitment to stalled forks, both of which are necessary for fork degradation in BRCA1/2-deficient cells.

It has been reported that restoration of fork protection confers chemoresistance to BRCA1/2-deficient cells (16). However, other reports suggest that fork protection does not confer chemoresistance of BRCA1/2-deficient cells (20,21). Our finding echoes the reports that restoration of fork protection does not lead to chemoresistance since the loss of CSB restores fork protection but fails to promote chemoresistance in BRCA1/2-deficient cells. In addition, both wild-type CSB and the CSB-T1031A mutant promote chemoresistance in BRCA2-depleted U2OS CSB-KO cells. While wild-type CSB promotes fork degradation in BRCA1/2-deficient cells, the CSB-T1031A mutant restores fork protection in these cells. These findings suggest that the status of fork protection is not necessarily correlated with chemosensitivity/chemoresistance in BRCA1/2-deficient cells.

It has been suggested that MRE11 promotes fork restart through both HR and BIR (61–63). We have previously reported that CSB promotes BRCA1-mediated HR (33). In this report, we have shown that CSB is not epistatic to BRCA1 in regulating BIR. CSB has been implicated in RAD52-dependent BIR (31). These findings suggest that it is likely that CSB promotes restart of stalled forks through both BRCA1-dependent HR and RAD52-dependent BIR in wild-type cells (Figure 8G). We envision that in BRCA1/2-deficient cells, CSB mediates RAD52-dependent BIR repair of DSBs arising from processing of stalled forks by MRE11 and MUS81, thereby promoting fork restart and cell survival upon replication stress (Figure 8G). This notion is in line with our finding that MRE11 and MUS81 mediate the excessive accumulation of cisplatin-induced chromatid breaks in BRCA1/2-deficient CSB-KO cells. In addition, CSB acts epistatically with RAD52 to prevent the excessive accumulation of cisplatin-induced chromatid breaks in BRCA1/2-deficient cells. Furthermore, the CSB-T1031A mutant, which is competent in preventing excessive accumulation of replication stress-induced chromatid breaks in BRCA1/2-deficient CSB-KO cells, promotes fork restart as well as cell survival in BRCA1/2-deficient CSB-KO cells upon replication stress. Our finding suggests that CSB is a promising target in the treatment of BRCA1/2-deficient cancer.

DATA AVAILABILITY

All data used in this study are available within the article and supplementary files or available from the authors upon request.

SUPPLEMENTARY DATA

Supplementary Data are available at NAR Online.

ACKNOWLEDGEMENTS

We would like to thank John Petrini for the MRE11 antibody, Roger Greenberg for U2OS-265 cells and Thanos Halazonetis for pBIR-GFP. S.Y.M. is a FRQS postdoctoral fellow. H.W. is a recipient of a Chercheur-Boursier Senior Scholarship from the Fonds Recherche Québec-Santé (FRQS). J.-Y.M. holds a Tier 1 Canada Research Chair in DNA Repair and Cancer Therapeutics.
Author contributions: N.L.B. performed the majority of the experiments. J.R.W. generated mammalian expression constructs of all CSB mutants. S.Y.M. and Y.C. performed

in vitro fork reversal assays and produced various recombinant CSB proteins as well as DNA substrates. I.H-M. assisted an experiment. J.R.W. conceived the project. J.R.W., J.-Y.M and X.-D.Z. designed the project with input from N.L.B. and S.Y.M. J.R.W. and X.-D.Z. wrote the paper with input from others.

FUNDING

Canadian Institutes of Health Research [PJT388346 to H.W., FDN-388879 to J.-Y.M., PJT159793 to X.-D.Z.]. Funding for open access charge: Canadian Institutes of Health Research.
Conflict of interest statement. None declared.

REFERENCES

1. Zeman,M.K. and Cimprich,K.A. (2014) Causes and consequences of replication stress. *Nat. Cell Biol.*, **16**, 2–9.
2. Gaillard,H., García-Muse,T. and Aguilera,A. (2015) Replication stress and cancer. *Nat. Rev. Cancer*, **15**, 276–289.
3. Berti,M. and Vindigni,A. (2016) Replication stress: getting back on track. *Nat. Struct. Mol. Biol.*, **23**, 103–109.
4. Atkinson,J. and McGlynn,P. (2009) Replication fork reversal and the maintenance of genome stability. *Nucleic Acids Res.*, **37**, 3475–3492.
5. Neelsen,K.J. and Lopes,M. (2015) Replication fork reversal in eukaryotes: from dead end to dynamic response. *Nat. Rev. Mol. Cell Biol.*, **16**, 207–220.
6. Taglialatela,A., Alvarez,S., Leuzzi,G., Sannino,V., Ranjha,L., Huang,J.W., Madubata,C., Anand,R., Levy,B., Rabadan,R. *et al.* (2017) Restoration of replication fork stability in BRCA1- and BRCA2-deficient cells by inactivation of SNF2-family fork remodelers. *Mol. Cell*, **68**, 414–430.
7. Kolinjivadi,A.M., Sannino,V., De Antoni,A., Zadorozhny,K., Kilkenny,M., Técher,H., Baldi,G., Shen,R., Ciccia,A., Pellegrini,L. *et al.* (2017) Smarcal1-mediated fork reversal triggers Mre11-dependent degradation of nascent DNA in the absence of Brca2 and stable Rad51 nucleofilaments. *Mol. Cell*, **67**, 867–881.
8. Betous,R., Mason,A.C., Rambo,R.P., Bansbach,C.E., Badu-Nkansah,A., Sirbu,B.M., Eichman,B.F. and Cortez,D. (2012) SMARCAL1 catalyzes fork regression and Holliday junction migration to maintain genome stability during DNA replication. *Genes Dev.*, **26**, 151–162.
9. Zellweger,R., Dalcher,D., Mutreja,K., Berti,M., Schmid,J.A., Herrandor,R., Vindigni,A. and Lopes,M. (2015) Rad51-mediated replication fork reversal is a global response to genotoxic treatments in human cells. *J. Cell Biol.*, **208**, 563–579.
10. Gari,K., Décaillet,C., Delannoy,M., Wu,L. and Constantinou,A. (2008) Remodeling of DNA replication structures by the branch point translocase FANCM. *Proc. Natl Acad. Sci. U.S.A.*, **105**, 16107–16112.
11. Vujanovic,M., Krietsch,J., Raso,M.C., Terraneo,N., Zellweger,R., Schmid,J.A., Taglialatela,A., Huang,J.W., Holland,C.L., Zwicky,K. *et al.* (2017) Replication fork slowing and reversal upon DNA damage require PCNA polyubiquitination and ZRANB3 DNA translocase activity. *Mol. Cell*, **67**, 882–890.
12. Blastyák,A., Hajdú,I., Unk,I. and Haracska,L. (2010) Role of double-stranded DNA translocase activity of human HLTF in replication of damaged DNA. *Mol. Cell. Biol.*, **30**, 684–693.
13. Nielsen,F.C., van Overeem Hansen,T. and Sorensen,C.S. (2016) Hereditary breast and ovarian cancer: new genes in confined pathways. *Nat. Rev. Cancer*, **16**, 599–612.
14. Mijic,S., Zellweger,R., Chappidi,N., Berti,M., Jacobs,K., Mutreja,K., Ursich,S., Ray Chaudhuri,A., Nussenzweig,A., Janscak,P. *et al.* (2017) Replication fork reversal triggers fork degradation in BRCA2-defective cells. *Nat. Commun.*, **8**, 859.
15. Lemaçon,D., Jackson,J., Quinet,A., Brickner,J.R., Li,S., Yazinski,S., You,Z., Ira,G., Zou,L., Mosammaparast,N. *et al.* (2017) MRE11 and EXO1 nucleases degrade reversed forks and elicit MUS81-dependent fork rescue in BRCA2-deficient cells. *Nat. Commun.*, **8**, 860.
16. Ray Chaudhuri,A., Callen,E., Ding,X., Gogola,E., Duarte,A.A., Lee,J.E., Wong,N., Lafarga,V., Calvo,J.A., Panzarino,N.J. *et al.* (2016) Replication fork stability confers chemoresistance in BRCA-deficient cells. *Nature*, **535**, 382–387.
17. Schlacher,K., Wu,H. and Jasin,M. (2012) A distinct replication fork protection pathway connects Fanconi anemia tumor suppressors to RAD51-BRCA1/2. *Cancer Cell*, **22**, 106–116.
18. Schlacher,K., Christ,N., Siaud,N., Egashira,A., Wu,H. and Jasin,M. (2011) Double-strand break repair-independent role for BRCA2 in blocking stalled replication fork degradation by MRE11. *Cell*, **145**, 529–542.
19. Ying,S., Hamdy,F.C. and Helleday,T. (2012) Mre11-dependent degradation of stalled DNA replication forks is prevented by BRCA2 and PARP1. *Cancer Res.*, **72**, 2814–2821.
20. Rickman,K.A., Noonan,R.J., Lach,F.P., Sridhar,S., Wang,A.T., Abhyankar,A., Huang,A., Kelly,M., Auerbach,A.D. and Smogorzewska,A. (2020) Distinct role of BRCA2 in replication fork protection in response to hydroxyurea and DNA interstrand cross-links. *Genes Dev.*, **34**, 832–846.
21. Panzarino,N.J., Krais,J.J., Cong,K., Peng,M., Mosqueda,M., Nayak,S.U., Bond,S.M., Calvo,J.A., Doshi,M.B., Bere,M. *et al.* (2021) Replication gaps underlie BRCA deficiency and therapy response. *Cancer Res.*, **81**, 1388–1397.
22. Hanada,K., Budzowska,M., Davies,S.L., van Drunen,E., Onizawa,H., Beverloo,H.B., Maas,A., Essers,J., Hickson,I.D. and Kanaar,R. (2007) The structure-specific endonuclease Mus81 contributes to replication restart by generating double-strand DNA breaks. *Nat. Struct. Mol. Biol.*, **14**, 1096–1104.
23. Regairaz,M., Zhang,Y.W., Fu,H., Agama,K.K., Tata,N., Agrawal,S., Aladjem,M.I. and Pommier,Y. (2011) Mus81-mediated DNA cleavage resolves replication forks stalled by topoisomerase I–DNA complexes. *J. Cell Biol.*, **195**, 739–749.
24. Costantino,L., Sotiriou,S.K., Rantala,J.K., Magin,S., Mladenov,E., Helleday,T., Haber,J.E., Iliakis,G., Kallioniemi,O.P. and Halazonetis,T.D. (2014) Break-induced replication repair of damaged forks induces genomic duplications in human cells. *Science*, **343**, 88–91.
25. Sotiriou,S.K., Kamileri,I., Lugli,N., Evangelou,K., Da-Ré,C., Huber,F., Padayachy,L., Tardy,S., Nicati,N.L., Barriot,S. *et al.* (2016) Mammalian RAD52 functions in break-induced replication repair of collapsed DNA replication forks. *Mol. Cell*, **64**, 1127–1134.
26. Lake,R.J., Geyko,A., Hemashettar,G., Zhao,Y. and Fan,H.Y. (2010) UV-induced association of the CSB remodeling protein with chromatin requires ATP-dependent relief of N-terminal autorepression. *Mol. Cell*, **37**, 235–246.
27. Batenburg,N.L., Walker,J.R., Noordermeer,S.M., Moatti,N., Durocher,D. and Zhu,X.D. (2017) ATM and CDK2 control chromatin remodeler CSB to inhibit RIF1 in DSB repair pathway choice. *Nat. Commun.*, **8**, 1921.
28. Troelstra,C., van Gool,A., de Wit,J., Vermeulen,W., Bootsma,D. and Hoeijmakers,J.H. (1992) ERCC6, a member of a subfamily of putative helicases, is involved in Cockayne's syndrome and preferential repair of active genes. *Cell*, **71**, 939–953.
29. van der Horst,G.T., van Steeg,H., Berg,R.J., van Gool,A.J., de Wit,J., Weeda,G., Morreau,H., Beems,R.B., van Kreijl,C.F., de Gruijl,F.R. *et al.* (1997) Defective transcription-coupled repair in Cockayne syndrome B mice is associated with skin cancer predisposition. *Cell*, **89**, 425–435.
30. Batenburg,N.L., Thompson,E.L., Hendrickson,E.A. and Zhu,X.D. (2015) Cockayne syndrome group B protein regulates DNA double-strand break repair and checkpoint activation. *EMBO J.*, **34**, 1399–1416.
31. Teng,Y., Yadav,T., Duan,M., Tan,J., Xiang,Y., Gao,B., Xu,J., Liang,Z., Liu,Y., Nakajima,S. *et al.* (2018) ROS-induced R loops trigger a transcription-coupled but BRCA1/2-independent homologous recombination pathway through CSB. *Nat. Commun.*, **9**, 4115.
32. Feng,E., Batenburg,N.L., Walker,J.R., Ho,A., Mitchell,T.R.H., Qin,J. and Zhu,X.D. (2020) CSB cooperates with SMARCAL1 to maintain telomere stability in ALT cells. *J. Cell Sci.*, **133**, jcs234914.
33. Batenburg,N.L., Walker,J.R., Coulombe,Y., Sherker,A., Masson,J.Y. and Zhu,X.D. (2019) CSB interacts with BRCA1 in late S/G2 to promote MRN- and CtIP-mediated DNA end resection. *Nucleic Acids Res.*, **47**, 10678–10692.
34. Scheibye-Knudsen,M., Mitchell,S.J., Fang,E.F., Iyama,T., Ward,T., Wang,J., Dunn,C.A., Singh,N., Veith,S., Hasan,M.M. *et al.* (2014) A high fat diet and NAD^+ rescue premature aging in Cockayne syndrome. *Cell Metab.*, **20**, 840–855.

35. Squires,S., Ryan,A.J., Strutt,H.L. and Johnson,R.T. (1993) Hypersensitivity of Cockayne's syndrome cells to camptothecin is associated with the generation of abnormally high levels of double strand breaks in nascent DNA. *Cancer Res.*, **53**, 2012–2019.
36. Enoiu,M., Jiricny,J. and Schärer,O.D. (2012) Repair of cisplatin-induced DNA interstrand crosslinks by a replication-independent pathway involving transcription-coupled repair and translesion synthesis. *Nucleic Acids Res.*, **40**, 8953–8964.
37. Batenburg,N.L., Qin,J., Walker,J.R. and Zhu,X.D. (2018) Efficient UV repair requires disengagement of the CSB winged helix domain from the CSB ATPase domain. *DNA Repair*, **68**, 58–67.
38. Batenburg,N.L., Mitchell,T.R., Leach,D.M., Rainbow,A.J. and Zhu,X.D. (2012) Cockayne syndrome group B protein interacts with TRF2 and regulates telomere length and stability. *Nucleic Acids Res.*, **40**, 9661–9674.
39. Zhang,H., Liu,H., Chen,Y., Yang,X., Wang,P., Liu,T., Deng,M., Qin,B., Correia,C., Lee,S. *et al.* (2016) A cell cycle-dependent BRCA1–UHRF1 cascade regulates DNA double-strand break repair pathway choice. *Nat. Commun.*, **7**, 10201.
40. Blessing,C., Mandemaker,I.K., Gonzalez-Leal,C., Preisser,J., Schomburg,A. and Ladurner,A.G. (2020) The oncogenic helicase ALC1 regulates PARP inhibitor potency by trapping PARP2 at DNA breaks. *Mol. Cell*, **80**, 862–875.
41. Tian,T., Bu,M., Chen,X., Ding,L., Yang,Y., Han,J., Feng,X.H., Xu,P., Liu,T., Ying,S. *et al.* (2021) The ZATT–TOP2A–PICH axis drives extensive replication fork reversal to promote genome stability. *Mol. Cell*, **81**, 198–211.
42. Chappidi,N., Nascakova,Z., Boleslavska,B., Zellweger,R., Isik,E., Andrs,M., Menon,S., Dobrovolna,J., Balbo Pogliano,C., Matos,J. *et al.* (2020) Fork cleavage–religation cycle and active transcription mediate replication restart after fork stalling at co-transcriptional R-loops. *Mol. Cell*, **77**, 528–541.
43. Zhu,X.D., Kuster,B., Mann,M., Petrini,J.H. and Lange,T. (2000) Cell-cycle-regulated association of RAD50/MRE11/NBS1 with TRF2 and human telomeres. *Nat. Genet.*, **25**, 347–352.
44. Wilson,F.R., Ho,A., Walker,J.R. and Zhu,X.D. (2016) Cdk-dependent phosphorylation regulates TRF1 recruitment to PML bodies and promotes C-circle production in ALT cells. *J. Cell Sci.*, **129**, 2559–2572.
45. Wu,Y., Xiao,S. and Zhu,X.D. (2007) MRE11–RAD50–NBS1 and ATM function as co-mediators of TRF1 in telomere length control. *Nat. Struct. Mol. Biol.*, **14**, 832–840.
46. Wu,Y., Mitchell,T.R. and Zhu,X.D. (2008) Human XPF controls TRF2 and telomere length maintenance through distinctive mechanisms. *Mech. Ageing Dev.*, **129**, 602–610.
47. Nieminuszczy,J., Schwab,R.A. and Niedzwiedz,W. (2016) The DNA fiber technique: tracking helicases at work. *Methods*, **108**, 92–98.
48. Buisson,R., Niraj,J., Pauty,J., Maity,R., Zhao,W., Coulombe,Y., Sung,P. and Masson,J.Y. (2014) Breast cancer proteins PALB2 and BRCA2 stimulate polymerase η in recombination-associated DNA synthesis at blocked replication forks. *Cell Rep.*, **6**, 553–564.
49. Shanbhag,N.M., Rafalska-Metcalf,I.U., Balane-Bolivar,C., Janicki,S.M. and Greenberg,R.A. (2010) ATM-dependent chromatin changes silence transcription in cis to DNA double-strand breaks. *Cell*, **141**, 970–981.
50. Batenburg,N.L., Cui,S., Walker,J.R. and Zhu,X.D. (2021) The winged helix domain of CSB regulates RNAPII occupancy at promoter proximal pause sites. *Int. J. Mol. Sci.*, **22**, 3379.
51. Robison,J.G., Elliott,J., Dixon,K. and Oakley,G.G. (2004) Replication protein A and the Mre11.Rad50.Nbs1 complex co-localize and interact at sites of stalled replication forks. *J. Biol. Chem.*, **279**, 34802–34810.
52. Roy,S., Luzwick,J.W. and Schlacher,K. (2018) SIRF: quantitative *in situ* analysis of protein interactions at DNA replication forks. *J. Cell Biol.*, **217**, 1521–1536.
53. Alabert,C., Bukowski-Wills,J.C., Lee,S.B., Kustatscher,G., Nakamura,K., de Lima Alves,F., Menard,P., Mejlvang,J., Rappsilber,J. and Groth,A. (2014) Nascent chromatin capture proteomics determines chromatin dynamics during DNA replication and identifies unknown fork components. *Nat. Cell Biol.*, **16**, 281–293.
54. Higgs,M.R., Reynolds,J.J., Winczura,A., Blackford,A.N., Borel,V., Miller,E.S., Zlatanou,A., Nieminuszczy,J., Ryan,E.L., Davies,N.J. *et al.* (2015) BOD1L is required to suppress deleterious resection of stressed replication forks. *Mol. Cell*, **59**, 462–477.
55. Przetocka,S., Porro,A., Bolck,H.A., Walker,C., Lezaja,A., Trenner,A., von Aesch,C., Himmels,S.F., D'Andrea,A.D., Ceccaldi,R. *et al.* (2018) CtIP-mediated fork protection synergizes with BRCA1 to suppress genomic instability upon DNA replication stress. *Mol. Cell*, **72**, 568–582.
56. Somyajit,K., Spies,J., Coscia,F., Kirik,U., Rask,M.B., Lee,J.H., Neelsen,K.J., Mund,A., Jensen,L.J., Paull,T.T. *et al.* (2021) Homology-directed repair protects the replicating genome from metabolic assaults. *Dev. Cell*, **56**, 461–477.
57. Bai,G., Kermi,C., Stoy,H., Schiltz,C.J., Bacal,J., Zaino,A.M., Hadden,M.K., Eichman,B.F., Lopes,M. and Cimprich,K.A. (2020) HLTF promotes fork reversal, limiting replication stress resistance and preventing multiple mechanisms of unrestrained DNA synthesis. *Mol. Cell*, **78**, 1237–1251.
58. Citterio,E., Rademakers,S., van der Horst,G.T., van Gool,A.J., Hoeijmakers,J.H. and Vermeulen,W. (1998) Biochemical and biological characterization of wild-type and ATPase-deficient Cockayne syndrome B repair protein. *J. Biol. Chem.*, **273**, 11844–11851.
59. Selby,C.P. and Sancar,A. (1997) Human transcription-repair coupling factor CSB/ERCC6 is a DNA-stimulated ATPase but is not a helicase and does not disrupt the ternary transcription complex of stalled RNA polymerase II. *J. Biol. Chem.*, **272**, 1885–1890.
60. Scheibye-Knudsen,M., Tseng,A., Borch Jensen,M., Scheibye-Alsing,K., Fang,E.F., Iyama,T., Bharti,S.K., Marosi,K., Froetscher,L., Kassahun,H. *et al.* (2016) Cockayne syndrome group A and B proteins converge on transcription-linked resolution of non-B DNA. *Proc. Natl Acad. Sci. U.S.A.*, **113**, 12502–12507.
61. Trenz,K., Smith,E., Smith,S. and Costanzo,V. (2006) ATM and ATR promote Mre11 dependent restart of collapsed replication forks and prevent accumulation of DNA breaks. *EMBO J.*, **25**, 1764–1774.
62. Bryant,H.E., Petermann,E., Schultz,N., Jemth,A.S., Loseva,O., Issaeva,N., Johansson,F., Fernandez,S., McGlynn,P. and Helleday,T. (2009) PARP is activated at stalled forks to mediate Mre11-dependent replication restart and recombination. *EMBO J.*, **28**, 2601–2615.
63. Hashimoto,Y., Puddu,F. and Costanzo,V. (2011) RAD51- and MRE11-dependent reassembly of uncoupled CMG helicase complex at collapsed replication forks. *Nat. Struct. Mol. Biol.*, **19**, 17–24.
64. Li,S., Wang,H., Jehi,S., Li,J., Liu,S., Wang,Z., Truong,L., Chiba,T., Wang,Z. and Wu,X. (2021) PIF1 helicase promotes break-induced replication in mammalian cells. *EMBO J.*, **40**, e104509.
65. Bunting,S.F., Callen,E., Wong,N., Chen,H.T., Polato,F., Gunn,A., Bothmer,A., Feldhahn,N., Fernandez-Capetillo,O., Cao,L. *et al.* (2010) 53BP1 inhibits homologous recombination in Brca1-deficient cells by blocking resection of DNA breaks. *Cell*, **141**, 243–254.
66. Minocherhomji,S., Ying,S., Bjerregaard,V.A., Bursomanno,S., Aleliunaite,A., Wu,W., Mankouri,H.W., Shen,H., Liu,Y. and Hickson,I.D. (2015) Replication stress activates DNA repair synthesis in mitosis. *Nature*, **528**, 286–290.
67. Pereira,B., Chin,S.F., Rueda,O.M., Vollan,H.K., Provenzano,E., Bardwell,H.A., Pugh,M., Jones,L., Russell,R., Sammut,S.J. *et al.* (2016) The somatic mutation profiles of 2,433 breast cancers refines their genomic and transcriptomic landscapes. *Nat. Commun.*, **7**, 11479.
68. Curtis,C., Shah,S.P., Chin,S.F., Turashvili,G., Rueda,O.M., Dunning,M.J., Speed,D., Lynch,A.G., Samarajiwa,S., Yuan,Y. *et al.* (2012) The genomic and transcriptomic architecture of 2,000 breast tumours reveals novel subgroups. *Nature*, **486**, 346–352.
69. Gao,J., Aksoy,B.A., Dogrusoz,U., Dresdner,G., Gross,B., Sumer,S.O., Sun,Y., Jacobsen,A., Sinha,R., Larsson,E. *et al.* (2013) Integrative analysis of complex cancer genomics and clinical profiles using the cBioPortal. *Sci. Signal.*, **6**, pl1.
70. Cerami,E., Gao,J., Dogrusoz,U., Gross,B.E., Sumer,S.O., Aksoy,B.A., Jacobsen,A., Byrne,C.J., Heuer,M.L., Larsson,E. *et al.* (2012) The cBio Cancer Genomics Portal: an open platform for exploring multidimensional cancer genomics data. *Cancer Discov.*, **2**, 401–404.
71. Rondinelli,B., Gogola,E., Yücel,H., Duarte,A.A., van de Ven,M., van der Sluijs,R., Konstantinopoulos,P.A., Jonkers,J., Ceccaldi,R., Rottenberg,S. *et al.* (2017) EZH2 promotes degradation of stalled replication forks by recruiting MUS81 through histone H3 trimethylation. *Nat. Cell Biol.*, **19**, 1371–1378.